Prom. Nr. 2195

The Secondary Flow in Curved Pipes

THESIS

PRESENTED TO

THE SWISS FEDERAL INSTITUTE OF TECHNOLOGY, ZURICH

FOR THE DEGREE OF DOCTOR OF TECHNICAL SCIENCES

BY

Ralph William Detra

Citizen of the United States of America

Accepted on the recommendation of

Prof. Dr. J. Ackeret and Prof. H. Gerber

Zürich 1953
Dissertationsdruckerei Leemann AG

Erscheint als Nr. 20 der Mitteilungen aus dem Institut für Aerodynamik
an der Eidgenössischen Technischen Hochschule in Zürich
Herausgegeben von Prof. Dr. J. Ackeret

Verlag Leemann Zürich

Preface

The following study of the secondary flow in curved pipes was made at the Institut für Aerodynamik der Eidgenössischen Technischen Hochschule in Zürich under the scientific direction of Professor Dr. J. Ackeret. The study includes an experimental investigation of the secondary flow phenomenon followed by a theoretical investigation of the initial or starting phases of the secondary flow in slightly bent pipes made through an application of the equations of motion of an incompressible inviscid fluid.

I would like to take this opportunity to express my indebtedness to Professor Dr. J. Ackeret for his most helpful suggestions and unfailing interest during the progress of this work, as well as the permission to use the experimental apparatus. Thanks are due also to Mr. Sprenger of the Institut für Aerodynamik for his assistance with the experimental equipment. I also want to acknowledge the financial support received, during this work, through a Fellowship granted by the National Research Council, Washington, D.C.

R. W. Detra

Leer - Vide - Empty

Contents

Chapter I: General Considerations 7
§ 1. Introduction 7
§ 2. Definition of Secondary Flow 8
§ 3. The Secondary Flow Phenomenon in Curved Pipes 8
§ 4. Previous Work on the Flow in Bends 12

Chapter II: Preliminary Theoretical Investigations 13
§ 1. The Vorticity Distribution and Stream Function 13

Chapter III: Experimental Investigations 18
§ 1. Introduction 18
§ 2. Experimental Apparatus 18
§ 3. Test Procedure and Results 21
A. Test Procedure 21
B. Experimental Results 21

Chapter IV: Theory for the Secondary Flow in Curved Pipes 25
§ 1. The General Problem 25
§ 2. A New Approach and its Solution for Circular Pipes 27
§ 3. The Relation between the Vorticity and the Axial Velocity 34
§ 4. The Theory for Elliptic Pipes 35

Chapter V: Application of the Theory 38

Chapter VI: The Losses Due to the Secondary Flow 44
§ 1. The Loss Coefficient and its Application 44
§ 2. The Loss in Circular and Elliptic Pipes 46

Appendix A: Convergence of the Method of Solution for the Secondary Flow . . . 48

Literature References 50

Definitions of the Important Symbols

r, φ, z = cylindrical coordinates

ρ, ϑ = polar coordinates as used in Chapter II

$\gamma(r, \varphi) = h(r) \cos \varphi$ = axial component of vorticity

r_1 = outside radius of circular cross-section

u = radial velocity component

v = tangential velocity component

w = axial velocity component

ψ = stream function

$\overline{w}$ = average mass-flow axial velocity

$Re = \dfrac{\overline{w} d}{\nu}$ = Reynolds Number

ρ = mass density

p = pressure

f = body force per unit mass

R = radius of curvature of the bent pipe

$\eta = \dfrac{r}{r_1}$ = dimensionless radius

w_0 = maximum value of the axial velocity

$\beta = \dfrac{w}{w_0}$ = dimensionless inlet-velocity distribution

$\delta = \dfrac{z}{r_1}$ = dimensionless distance from the inlet of curved pipe

$\lambda = \dfrac{r_1}{R}$ = dimensionless ratio of radii

$\theta = \lambda \delta$ = angle of bend of the curved pipe

$\sigma(\eta) \cos \varphi = \dfrac{\psi}{\lambda \delta r_1 w_0}$ = dimensionless secondary flow stream function

ξ, φ, z = elliptic cylindrical coordinates

a, b = semi-major and -minor axes of the elliptic cross-section

ζ = secondary flow loss coefficient

Chapter I. General Considerations

§ 1. Introduction

The goal of every engineer is to always improve the efficiency and performance of the machines and equipment he designs. In order to do so it is important to understand the phenomena and processes associated with these machines. As a result of this understanding, the sources of the losses and inefficiencies can more easily be found, and subsequently their magnitudes and effects evaluated.

It has been known for some time that when fluid with a non-uniform velocity flows in a curved pipe, there arise losses which are greater than those for the corresponding length of straight pipe. Therefore, there must be a phenomenon present in the flow in a bend, which is not present in a straight pipe, from which these losses originate. Another consequence of this phenomenon is that it distorts the shape of the axial-velocity distribution as the flow moves around the bend of the pipe. To obtain a knowledge, about this flow in a curved pipe, is desirable and important from both the scientific and practical view-points. It was, thus, the purpose of this investigation to obtain an understanding of the flow processes involved, and subsequently to develop a theory for predicting these processes. Recognizing the undisputed value of having a physical comprehension of a problem, the investigation was carried out using, where possible, a close connection between physics and theory.

Applications of the results of an investigation of the flow in curved pipes are rather apparent. For example, the airplane, which today shows, indeed, a great improvement in performance and efficiency over those of the previous decade, still offers opportunities for improvements. Its overall efficiency is, of course, determined by the efficiencies of its various components, which with the complexity of the present-day airplane are numerous. Herein lie the possibilities of an application of this information. It can be used to good advantage in the design of the many flow passages used to conduct air from one place to another within the airplane, for example the air intakes to the engines. In addition, the advent of the turbo-jet and rocket engines, as applied to airplanes, has opened many fields where the knowledge about flow in curved passages and pipes is a necessity if these machines are to be designed for maximum efficiency. To be sure, the information can be applied to stationary machines as well, the airplane being simply one example.

In the following work a study is made of the fluid flow in a curved pipe. Discussed first from a physical point of view, a basis for the origin of the phenomenon which arises is suggested. The results of experiments on the flow in curved pipes, which were conducted at the Institut für Aerodynamik der E.T.H., Zürich, support this physical argument, thus indicating that the deductions are sound. Drawing on the above information, a first order theory is developed to predict the flow phenomenon in a curved pipe whose cross-

sectional dimensions are small compared to its radius of curvature and whose angle of bend is small. As such, the theoretical study is a study of the initial phases of the secondary flow phenomenon in a curved pipe. An application of this theory is then made, the results of which are compared with the results of the above mentioned experiments.

§ 2. Definition of Secondary Flow

Many basic fluid-motion studies are made by assuming that the motion is irrotational. Irrotational motion is defined by that motion for which the curl of the velocity vector is zero. The curl of the velocity vector is called the vorticity, which is defined physically as twice the angular velocity of the fluid particle. Irrotational motion is equivalent to or constitutes motion free of vorticity. Since the curl of every gradient is identically zero, it is possible, when irrotational motion exists, to write the velocity vector as the gradient of a scalar function. This scalar function is called the potential function and the motion that exists under these conditions is called potential flow. The necessary as well as the sufficient condition that must be satisfied in order to have a potential flow is that the flow be irrotational. Restricted to the consideration of an incompressible fluid, the differential equation satisfied by the potential function is Laplace's equation. From this one scalar potential function the three mutually perpendicular velocity components of a general flow problem can be found and thus an extreme simplification has been achieved. Much attention in the past has been given to the problem of finding solutions of Laplace's equation as applied to fluid motion. The general problem of solving Laplace's equation, which constitutes Potential Theory, is the subject of a great literature. The irrotational assumption is also equivalent to saying that the stagnation pressure is the same along all streamlines, in fact throughout the whole flow field.

In practice, however, it often happens that the stagnation pressure is not the same along all streamlines, but varys slightly from one streamline to another. This then means the flow is not irrotational but only approximately so, and hence the definition of a scalar potential function for the flow is impossible. The difference between the potential flow and this approximately potential flow in the normal plane is called secondary flow. Consequently the secondary flow must contain vorticity. This vorticity, in turn, constitutes a motion of the fluid particles, which is not necessarily restricted to involve motion of the fluid particles along the streamlines of the potential flow, but can define other streamlines. If this difference, which describes the secondary flow, is small, then it is conceivable that the velocities and, subsequently, the losses of this secondary flow are correspondingly small.

§ 3. The Secondary Flow Phenomenon in Curved Pipes

According to the definition of secondary flow there arises a vorticity in the flow field. Since the vorticity is defined mathematically as being equal to the curl of the velocity vector, this vorticity must arise from a velocity gradient. It is clear that a non-uniform axial-velocity distribution in a straight pipe will produce vorticity in the flow due to the non-uniform distribution. If this flow

then moves around a curve in the pipe this vorticity will still be present, so that it cannot be considered as a result of the effects of the bend itself. Since we are interested in the phenomena caused by the bend itself we must therefore ask if there is any other possible source in a curved pipe flow, which could provide an origin of the vorticity in the secondary flow. We shall therefore investigate the possibility of whether a non-uniform velocity distribution and subsequentily a vorticity distribution can originate in the cross-section of the pipe perpencicular to its longitudinal axis.

Consider now simply a fluid flow moving in a curved path. Each particle of the fluid, as it moves in the curved path, is acted upon by a centrifugal force. The definition of a fluid particle as used here is a very small element of mass of the fluid which still displays the general characteristic properties of a large sample of the fluid. This assumes the fluid is continuous and homogenous in structure. From the results of mechanics of solid bodies, we know the centrifugal force, present during curvilinear motion of a body, is directly proportional to the square of the body's velocity and indirectly proportional to the radius of curvature of its path. Drawing an analogy from this result, the centrifugal force acting on each fluid particle is taken to be directly proportional to the square of the particle's velocity and indirectly proportional to the radius of curvature of its path. It must be emphasized, however, that since the fluid is considered as a continuum, each fluid particle cannot be treated itself as a solid body. During a fluid motion every particle, as considered here, is being deformed continually and hence it does not satisfy the requirement of the definition of a solid body. Also, since the fluid particles are, in fact, touching each other, the motion of one will influence the motion of the others within the fluid region. Under the action of this centrifugal force each of the fluid particles is forced toward the outside of the curved path in the direction of a line drawn through the path from the center of curvature of the path.

Now by applying this information to the flow in a curved pipe, the origin of the secondary flow in a plane perpendicular to the longitudinal axis of the pipe can be seen. Under the condition of a non-uniform axial-velocity distribution, the centrifugal forces acting on the fluid particles within the cross-section of the pipe are clearly of different magnitude. These centrifugal forces acting in the plane of the pipe perpendicular to its longitudinal axis then create a motion of the fluid particles in this plane. The fluid particles with the higher axial velocity are acted upon by a larger centrifugal force than the slower moving particles. Thus if the size of the particles is chosen such that the mass of every particle is the same, the particles having the higher axial velocity will have a correspondingly higher velocity within the cross-section of the pipe, due to the centrifugal forces. The resulting motion will then have a non-uniform velocity distribution within the cross-section of the pipe, giving rise to a vorticity in this plane and thus satisfying our definition of a secondary flow.

Having concluded that the flow in a curved pipe provides the necessary source for the origin of a secondary flow, it is of interest to investigate the consequences of this secondary flow. Consider the flow in a curved circular pipe, with an inlet stagnation-pressure distribution, which is symmetrical about the longitudinal axis of the cross-section (see Fig. 1).

The fluid particles in the center of the pipe will be forced harder, under the action of the centrifugal force, to move toward the outside of the bend than

the particles which are located in the region closer to the wall, i.e. the lower velocity region. So as the higher stagnation-pressure particles move toward the outside of the bend, they displace the particles with the lower stagnation pressure. Since the cross-section of the pipe is closed and since the continuity conditions within the cross-section must be satisfied, the lower stagnation-pressure particles will be forced to move along the wall of the pipe toward the

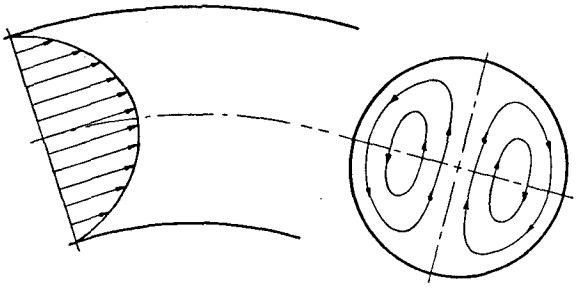

Fig. 1. The streamlines of the secondary flow in a curved circular pipe resulting from a symmetrical inlet stagnation-pressure distribution.

inside of the bend. This motion, set up by the outward movement of the particles with the higher stagnation pressure and the simultaneous movement of the lower stagnation-pressure particles along the wall of the pipe toward the inside of the bend, constitutes the secondary flow.

The shape of the streamlines, as shown in Fig. 1, resulting from such a motion in a circular pipe, resemble the streamlines due to a vortex pair located inside of a circular cylinder.

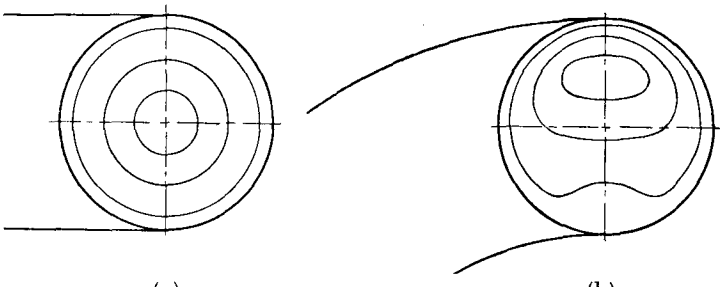

(a) (b)

Fig. 2. Lines of constant stagnation pressure at: (a), the entrance and (b), within the bend of a curved pipe.

One of the primary effects of this secondary motion is to change the shape of the stagnation-pressure distribution. For discussional purposes, let us say that the inlet stagnation-pressure distribution of a flow in a curved circular pipe is symmetrical about the pipe's longitudinal axis. A plot of the lines of constant stagnation pressure at the entrance is a system of concentric circles (Fig. 2), the smaller circles indicating the higher velocity in the central region of the pipe and the larger circles indicating the lower velocities. At a section

in the bend of the pipe, that is after a given angular displacement of the fluid, a secondary motion of the fluid particles will have arisen and subsequently affected the shape of the stagnation-pressure profile. The result is that the lines of constant stagnation pressure, which were circles at the inlet, are no longer circles. The curves defining the constant stagnation-pressure regions will have moved toward the outside of the bend and at the same time will have been distorted in shape. The portions of the curves toward the outside of the bend assume, in general, the cross-sectional shape of the pipe, in this case a circle. However, the portions of the curves toward the inside of the bend, being affected by the reverse flow of the fluid along the wall of the pipe, are, in general, flattened and may exhibit the indentations as shown in Fig. 2. Under the conditions of a symmetrical inlet stagnation-pressure distribution, as discussed here, it is expected that the resulting secondary motion will be symmetrical about the diameter of the pipe drawn in the plane of the bend. Therefore, the lines of constant stagnation pressure will also be symmetrical about this line.

Another consequence of the secondary flow is that it represents a loss. Clearly, if no secondary motion exists in the inlet flow but in the bend a secondary motion does exist, it means energy must have been supplied from some available source to promote this motion. In this case, the source of energy is the kinetic energy of the axial fluid motion plus the work of the entrance surface forces. The energy in the secondary flow represents a definite dissipation, unless it is recovered by some useful means.

For the flow in a curved pipe whose angle of bend is large, the limiting case being where the bend angle tends toward infinity, it is conceivable that the secondary flow also tends toward a stationary state where it is no longer dependent on the bend angle. This situation can be pictured as follows: Within the bend the centrifugal force will always be present and will produce the effects discussed above. If this were the only phenomenon present one would believe that after all the fluid particles with the higher stagnation pressure were forced toward the outside of the bend the secondary motion would cease. However, acting simultaneously are the viscous forces whose effects permit an explanation supporting the contention that the secondary motion continues. As we have seen, the effect of the centrifugal force is to cause an increase in the stagnation-pressure gradient on the outside of the bend. With respect to the viscous forces this increased gradient corresponds to an increase in dissipation. This increase in dissipation on the outside of the bend would cause a decrease in the stagnation pressure of these fluid particles, resulting once again in a stagnation-pressure distribution where the greater stagnation pressure is in the central region of the pipe. This corresponds to the initial conditions used to discuss the effects of the centrifugal force and so under the action of the centrifugal force these higher stagnation-pressure fluid particles in the central region of the pipe would be forced to move toward the outside of the bend thus repeating the process described. When the simultaneous effects of the centrifugal force and the dissipation come into balance, the secondary motion will be independent of the bend angle, but a secondary fluid flow will exist. This type of secondary flow, which is independent of the bend angle, is called fully developed bend flow. Clearly, the transition of the secondary motion from its initial phases to fully developed bend flow progresses more rapidly as the effect of the viscosity increases.

Since we are interested in the initial phases of the secondary flow, the assumption of no dependence on the bend angle, i.e. fully developed bend flow, is not made. Therefore, the results of the following investigation show a dependence on the bend angle of the pipe.

§ 4. Previous Work on the Flow in Bends

The existence of the secondary flow which occurs in bends has been known for some time. *Thomson* [1]*) discussed it from the standpoint of the flow in the bends of rivers. With the respect to the flow in curved pipes it was realized that curved pipes have a greater pressure drop than the corresponding length of straight pipe. It was then deduced that perhaps these losses which occur could be related to the geometry of the pipes and the Reynolds number of the flow. Consequently early experimentors were interested only in defining a bend loss coefficient as a function of various parameters. The ultimate goal being that of proposing an empirical equation for predicting the losses and of finding design possibilities for minimizing these losses. On the other hand, theoretical investigations, starting with the equations of motion, to predict the secondary flows in curved pipes and their losses from a purely theoretical basis have been relatively few.

Dean [2] made a theoretical study of the viscous flow in a bent circular pipe, assuming fully developed bend flow, so that the solution is the same in every cross-section of the bend. The equations of motion, obtained by assuming the ratio of the radius of curvature of the bend to the diameter of the pipe is large compared to one, are solved by an expansion about the Reynolds number. The convergence of the solution restricts it to Reynolds numbers smaller than approximately 400. For this region of application of his theory, he found the resistance in a curved pipe to be a function of the parameter $Re\left(\frac{a}{R}\right)^{1/2}$, where Re is the Reynolds number and $\frac{a}{R}$ the ratio of the pipe radius to the radius of curvature of the bend. In a series of tests using both oil and water as the flow medium, *White* [3] confirmed this functional relation between the resistance and the parameter $Re\left(\frac{a}{R}\right)^{1/2}$. Later, *Adler* [4] also studied the laminar flow in bent circular pipes using the same approximation concerning the radius of curvature and the pipe diameter as *Dean*. His solution, resulting from an application of the Prandtl boundary-layer theory, is valid for large Reynolds numbers in the laminar flow region. The results of this theory also show that the resistance of a bent pipe is a function of the parameter $Re\left(\frac{a}{R}\right)^{1/2}$.

Nippert [5], [6] and *Richter* [7] conducted extensive tests on curved pipes with circular and rectangular cross-sections. In particular, investigations were made to determine the loss in the pipes as dependent on the various factors determining the geometry of the cross-section and the bend. *Wasielewski* [8] investigated the secondary flow losses in the bend of a circular pipe as a function of the bend angle. The measured losses, which include the secondary flow effects between the station 9 diameters upstream and the station 50 diameters downstream of the bend, indicate the secondary flow losses are a linear func-

*) The numbers in square brackets refer to the Literature References.

tion of the bend angle up to a bend of $22^1/_2$ degrees. *Taylor* [9], in an experimental study of the secondary flow phenomenon, showed visually the presence of the circulation in the cross-section of a circular pipe. This was done by injecting colored fluid through a small hole in the wall of a coiled glass pipe and then observing the motion of the colored fluid under the effect of the secondary flow. The motion of the colored fluid in the plane of the cross-section followed paths similar to the secondary flow streamlines suggested in § 3.

A more recent theoretical study was made by *Squire* and *Winter* [10], who, by neglecting viscosity developed a theory for the secondary flow in a cascade of airfoils with a non-uniform approach velocity. Their approach to the problem is made from channel flow considerations rather than using the Prandtl wing theory. *Hawthorne* [11] analyzed the flow in a bent circular pipe with an entrance velocity distribution which varies in only one direction, that is it varies linearly across the cross-section. He found this flow gives rise to a spiral motion of the fluid in the bend. The differential equation obtained for the fluid motion is analogous to the equation of motion of a pendulum, hence the theory predicts that the spiral motion is oscillatory as the flow moves around the bend. *Eichenberger* [12] found, from tests in a 90 degree bend of rectangular cross-section, that the streamline pattern appeared to be only slightly changed by a change in the Reynolds number. He also found that, of the total loss, approximately one half occurs within the bend and the other half occurs downstream of the bend. His measurements of the secondary flow velocities after a bend angle of 90 degrees indicate that the energy in the secondary flow is relatively small.

Chapter II. Preliminary Theoretical Investigations

§ 1. The Vorticity Distribution and Stream Function

According to the definition of secondary flow, the fluid motion is not irrotational but contains vorticity. The discussion of the secondary flow phenomenon in a circular pipe from the physical stand-point led to the deduction that the resulting secondary flow streamlines resembled those of a vortex pair located inside of a circular cylinder. However, it was also deduced that the source of the secondary flow, namely the axial-velocity gradient, is distributed over the cross-section of the pipe rather than being concentrated at two points as is the case for a vortex pair. This suggests that the streamlines of the secondary flow corresponds to those of a distribution of vortices over the cross-section. The question that then arises is: What vorticity distribution produces streamlines of this shape? A knowledge of the general form of this distribution and the resulting stream function will be helpful in a theoretical analysis of the secondary flow, which is made through an application of the equations of motion.

Considering a plane circular cylinder, the problem then is to find the stream function due to a system of vortices distributed over a region bounded by a circle. Let the radius of this plane circular region be denoted by r_1 and the strength of the infinitesimal vortices be denoted by $\gamma(\rho, \vartheta)$ where ρ and ϑ, the

usual polar coordinates, indicate the strength of the vortices is a variable depending on the location of the vortex. In order to satisfy the boundary condition that the circle of radius r_1 be a streamline, each vortex of strength γ, located inside the circle at the point (ρ, ϑ), must be accompanied by its image vortex of strength $-\gamma$, located at the image point $\left(\frac{r_1^2}{\rho}, \vartheta\right)$, [13]. Thus in calculating the velocity components at any point (r, φ), the contribution of each vortex plus its image must be taken in consideration.

For the motion of an inviscid incompressible fluid, the polar velocity components induced at the point (r, φ) by an infinitesimal vortex of strength γ located at the point (ρ, ϑ) are given by the equations, [14]

$$\delta u(r, \varphi) = -\frac{\gamma(\rho, \vartheta)}{2\pi} \frac{1}{r'} \sin \alpha \, \delta A$$

$$\delta v(r, \varphi) = +\frac{\gamma(\rho, \vartheta)}{2\pi} \frac{1}{r'} \cos \alpha \, \delta A$$

where the δu and δv indicates that these velocity components are only the contribution of an infinitesimal vortex. The length r' is the distance between the vortex and the point (r, φ) and δA is the area covered by the vortex. The angle α is defined in Fig. 3. In order to obtain the final velocity at any point

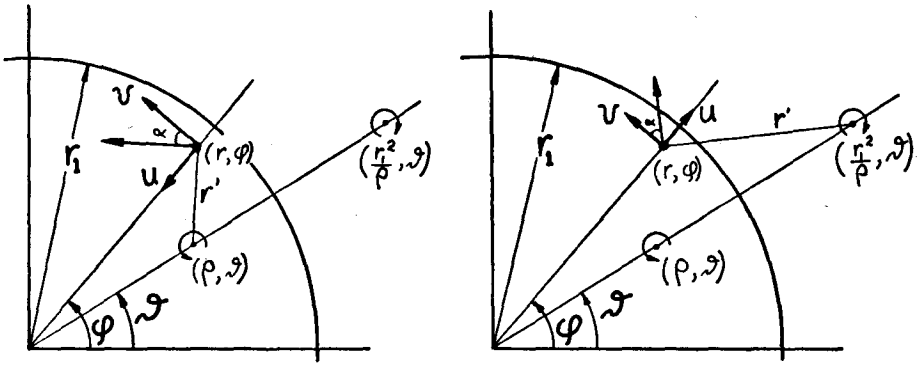

Fig. 3. The velocity components induced at a point (r, φ) by a vortex located inside a circle of radius r_1 at (ρ, ϑ), (a); and its image vortex located at $\left(\frac{r_1^2}{\rho}, \vartheta\right)$, (b).

(r, φ), the above equations must be summed over the entire distribution of vortices within the circle and the corresponding system of image vortices. As the position of the vortices within the circle vary from $\rho = r_1$ to $\rho = 0$ the position of the corresponding image vortices vary from $\frac{r_1^2}{\rho} = r_1$ to $\frac{r_1^2}{\rho} = \infty$, thus this summation must be carried out over the entire plane.

By evaluating r', $\sin \alpha$ and $\cos \alpha$ from the geometry shown in Fig. 3, the total velocity components due to the whole system of vortices and images are given by

$$u(r,\varphi)=\frac{-1}{2\pi}\int_0^{r_1} d\rho \int_0^{2\pi} \frac{\gamma(\rho,\vartheta)\sin(\varphi-\vartheta)\rho^2 d\vartheta}{r_a^2}+\frac{r_1^2}{2\pi}\int_0^{r_1} d\rho \int_0^{2\pi} \frac{\gamma(\rho,\vartheta)\sin(\varphi-\vartheta)\,d\vartheta}{r_b^2} \quad (1\text{a})$$

and

$$v(r,\varphi)=+\frac{1}{2\pi}\int_0^{r_1} d\rho \int_0^{2\pi} \frac{\gamma(\rho,\vartheta)[r-\rho\cos(\varphi-\vartheta)]\rho\, d\vartheta}{r_a^2}+\frac{1}{2\pi}\int_0^{r_1} d\rho \int_0^{2\pi} \frac{\gamma(\rho,\vartheta)[r_1^2/\rho\cos(\varphi-\vartheta)-r]\rho\, d\vartheta}{r_b^2}, \quad (1\text{b})$$

where

$$r_a^2 = r^2+\rho^2-2r\rho\cos(\varphi-\vartheta); \quad r_b^2 = r^2+\left(\frac{r_1^2}{\rho}\right)^2-2r\frac{r_1^2}{\rho}\cos(\varphi-\vartheta).$$

The consideration of the case with a symmetrical entrance-velocity distribution led to the deduction that the secondary flow streamlines are symmetrical about the diameter of the pipe lying in the plane of the curve. This then requires that the secondary flow velocities display a symmetry within the cross-section and hence also the secondary flow stream function. We therefore choose the distribution of the vortices within the circular region to be given by

$$\gamma(\rho,\vartheta) = h(\rho)\cos\vartheta. \quad (2)$$

Substitution of this relation into (1a) and (1b) yields the following equations:

$$u(r,\varphi)=\frac{-1}{2\pi}\int_0^{r_1} \rho^2 h(\rho)\,d\rho \int_0^{2\pi} \frac{\cos\vartheta\sin(\varphi-\vartheta)\,d\vartheta}{r_a^2}+\frac{r_1^2}{2\pi}\int_0^{r_1} h(\rho)\,d\rho \int_0^{2\pi} \frac{\cos\vartheta\sin(\varphi-\vartheta)\,d\vartheta}{r_b^2} \quad (3\text{a})$$

$$v(r,\varphi)=+\frac{1}{2\pi}\int_0^{r_1} \rho h(\rho)\,d\rho \int_0^{2\pi} \frac{\cos\vartheta[r-\rho\cos(\varphi-\vartheta)]\,d\vartheta}{r_a^2}+\frac{1}{2\pi}\int_0^{r_1} \rho h(\rho)\,d\rho \int_0^{2\pi} \frac{\cos\vartheta[r_1^2/\rho\cos(\varphi-\vartheta)-r]\,d\vartheta}{r_b^2} \quad (4\text{a})$$

If the assumed relation for the vorticity distribution (2) is correct, then the integration of (3a) and (4a) will yield the desired velocity components for obtaining streamlines of the general form as suggested in Chapter I. The integration with respect to the variable ϑ can be carried out immediately.

We consider first the integration of (3a). A substitution of the form $\varphi-\vartheta=\psi$ into the first integral with respect to ϑ yields the following two simplier integrals

$$\int_0^{2\pi} \frac{\cos\vartheta\sin(\varphi-\vartheta)\,d\vartheta}{r_a^2} = -\frac{1}{r^2+\rho^2}\left\{\cos\varphi\int_{\varphi}^{\varphi-2\pi}\frac{\sin\psi\cos\psi\,d\psi}{1-\epsilon\cos\psi}+\sin\varphi\int_{\varphi}^{\varphi-2\pi}\frac{\sin^2\psi\,d\psi}{1-\epsilon\cos\psi}\right\} \quad (3\text{b})$$

where $\epsilon = \dfrac{2\rho r}{r^2+\rho^2}$.

It can be shown that the first integral on the right hand side of (3b) is zero. The second integral can be further simplified by making the half angle substitution

$$t = \tan\frac{\psi}{2}; \qquad d\psi = \frac{2\,dt}{1+t^2}.$$

Upon making this substitution the second integral of (3b) becomes

$$\int_{\varphi}^{\varphi-2\pi} \frac{\sin^2\psi\, d\psi}{1-\epsilon\cos\psi} = \frac{8}{1+\epsilon} \int_{t(\varphi)}^{t(\varphi-2\pi)} \frac{t^2\, dt}{(1+t^2)^2(\zeta+t^2)}$$

where ζ is defined by $\zeta = \frac{1-\epsilon}{1+\epsilon}$. This integral with respect to t can be expanded by partial fractions in the following three simple integrals:

$$\int_{\varphi}^{\varphi-2\pi} \frac{\sin^2\psi\, d\psi}{1-\epsilon\cos\psi} = \frac{8}{1+\epsilon}\left\{\frac{\zeta}{(\zeta-1)^2}\int_{t(\varphi)}^{t(\varphi-2\pi)} \frac{dt}{1+t^2} - \frac{1}{\zeta-1}\int_{t(\varphi)}^{t(\varphi-2\pi)} \frac{dt}{(1+t^2)^2} - \frac{\zeta}{(\zeta-1)^2}\int_{t(\varphi)}^{t(\varphi-2\pi)} \frac{dt}{\zeta+t^2}\right\}. \quad (3c)$$

The integrals on the right hand side of (3c) are easily evaluated [15] yielding the result

$$\int_{\varphi}^{\varphi-2\pi} \frac{\sin^2\psi}{1-\epsilon\cos\psi}\, d\psi = -2\pi\left\{\frac{1-\sqrt{1-\epsilon^2}}{\epsilon^2}\right\}. \quad (3d)$$

At this point of the calculation distinction must be made between two possible cases. If the vortex under consideration is closer to the origin than the point at which we are calculating the radial velocity caused by the vortex, that is $\rho < r$, the term $\sqrt{1-\epsilon^2}$ gives the result $\frac{r^2-\rho^2}{r^2+\rho^2}$. The other case is when the vortex is further from the origin than the point (r, φ) so that $r < \rho$. Then the term $\sqrt{1-\epsilon^2}$ results in $\frac{\rho^2-r^2}{r^2+\rho^2}$. Using these facts, the value of the integral (3d) becomes

$$\int_{\varphi}^{\varphi-2\pi} \frac{\sin^2\psi\, d\psi}{1-\epsilon\cos\psi} = \begin{cases} -\pi\,\dfrac{r^2+\rho^2}{r^2}; & \rho < r \\ -\pi\,\dfrac{r^2+\rho^2}{\rho^2}; & \rho > r\,. \end{cases} \quad (3e)$$

We can thus write the result of the integration indicated by (3b) as

$$\int_0^{2\pi} \frac{\cos\vartheta\sin(\varphi-\vartheta)\, d\vartheta}{{r_a}^2} = \begin{cases} \dfrac{\pi\sin\varphi}{r^2}; & \rho < r \\ \dfrac{\pi\sin\varphi}{\rho^2}; & \rho > r\,. \end{cases} \quad (3f)$$

The integration of the second integral of (3a) with respect to ϑ is made in the following manner. The substitution $\varphi - \vartheta = \psi$ produces the two integrals

$$\int_0^{2\pi} \frac{\cos\vartheta\sin(\varphi-\vartheta)\, d\vartheta}{{r_b}^2} = -\frac{1}{r^2+\left(\frac{{r_1}^2}{\rho}\right)^2}\left\{\cos\varphi\int_{\varphi}^{\varphi-2\pi} \frac{\cos\psi\sin\psi\, d\psi}{1-\tau\cos\psi} + \sin\varphi\int_{\varphi}^{\varphi-2\pi} \frac{\sin^2\psi\, d\psi}{1-\tau\cos\psi}\right. \quad (3g)$$

where $\tau = \dfrac{2r\frac{{r_1}^2}{\rho}}{r^2+\left(\frac{{r_1}^2}{\rho}\right)^2}$.

The first integral on the right hand side of (3g), like that one of (3b), is zero. The second integral being similar to the second integral of (3b) is evaluated in a like fashion using the half angle substitution. However, since the integral (3g) gives the contribution of the image vortices, which are all located outside the circular region, only one value for the integral is obtained. It is

$$\int_0^{2\pi} \frac{\cos\vartheta \sin(\varphi-\vartheta)\, d\vartheta}{r_b^{\,2}} = \frac{\pi \sin\varphi}{\left(\frac{r_1^{\,2}}{\rho}\right)^2}. \tag{3h}$$

Using the results of the integrals (3f) and (3h), the radial velocity due to this system of vortices becomes

$$u(r,\varphi) = \frac{\sin\varphi}{2}\left\{\frac{1}{r_1^{\,2}}\int_0^{r_1} \rho\, h(\rho)\, d\rho - \frac{1}{r^2}\int_0^{r} \rho^2 h(\rho)\, d\rho - \int_r^{r_1} h(\rho)\, d\rho\right\}. \tag{3i}$$

The integration of the integrals for evaluating the tangential velocity (4a) is done in a similar manner, resulting in the following equation.

$$v(r,\varphi) = \frac{\cos\varphi}{2}\left\{\frac{1}{r^2}\int_0^{r} \rho^2 h(\rho)\, d\rho + \frac{1}{r_1^{\,2}}\int_0^{r_1} \rho^2 h(\rho)\, d\rho - \int_r^{r_1} h(\rho)\, d\rho\right\}. \tag{4b}$$

So if the vortex distribution $h(\rho)$ as a function of the radius is known the values of the polar velocities at any point (r,φ) due to this distribution of vortices can easily be found.

We now investigate a simple case by choosing the radial vortex distribution $h(\rho)$ as a linear function of the radius, i.e.

$$h(\rho) = k\rho.$$

Substitution of this vorticity distribution into equations (3i) and (4b) allows the evaluation of the polar velocity components which yields

$$u(r,\varphi) = \frac{k}{8}(r^2 - r_1^{\,2})\sin\varphi \tag{5}$$

and

$$v(r,\varphi) = \frac{k}{8}(3r^2 - r_1^{\,2})\cos\varphi\,. \tag{6}$$

We introduce a stream function defined by the relations

$$u = \frac{1}{r}\frac{\partial\psi}{\partial\varphi} \quad \text{and} \quad v = -\frac{\partial\psi}{\partial r}$$

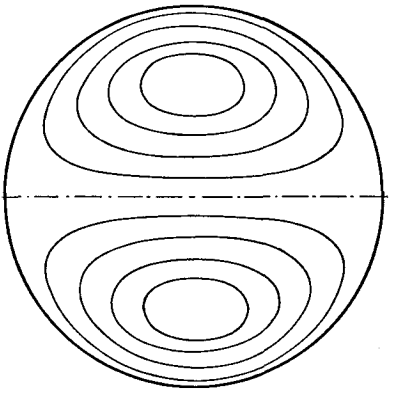

Fig. 4. The streamlines due to a distribution of vortices over the surface of a bounded circular area. The distribution of the vortices is given by $\gamma(\rho,\vartheta) = k\rho\cos\vartheta$.

from which, by using the values of the velocity components as given by (5) and (6), the stream function can be found as

$$\psi = \frac{k r}{8} (r_1^2 - r^2) \cos \varphi + \text{Const.} \tag{7}$$

A plot of the streamlines given by (7) is shown in Fig. 4. We see that the streamlines do exhibit the same general shape as those predicted by the physical conjectures of Chapter I. This then suggests that the stream function of the secondary flow, as obtained from an analysis made through an application of the equations of motion, should have the same general form of equation (7). In particular, the stream function should appear, for a given bend angle, as a trigonometric function of the polar angle times a functional dependence on the radius of the cross-section. In this analysis the functional dependence of the vorticity distribution on the radius of the cross-section is arbritary. From the previous discussion of the origin of the secondary flow in curved pipes, it is believed that the inlet stagnation-pressure distribution plays a predominant role. This then suggests that the inlet stagnation-pressure distribution will exert a strong influence in determining the radial dependence of the vorticity distribution and hence the secondary flow velocities and stream function.

Chapter III. Experimental Investigations

§ 1. Introduction

Experiments were conducted at the Institut für Aerodynamik, E. T. H., Zürich, to investigate the secondary flow, which arises when fluid flows in a curved pipe. For this investigation of the starting phases of the secondary flow, the experimental tests were conducted on curved constant-area circular pipes with a small ratio of diameter to radius of curvature as compared to one and a small angle of bend. To obtain a visualization of the effect of the bend and subsequently the secondary flow in changing the stagnation pressure distribution, these distributions were measured at the inlet and the exit of the curved pipes. Wall pressure measurements made along the length of the pipes and at different locations on the circumference of the cross-section show the variation of the wall static pressure as the flow expands to atmospheric pressure at the exit of the pipe.

§ 2. Experimental Apparatus

The flow medium used for these experiments was air. It was supplied from an electric-motor-driven centrifugal compressor, which exhausted the air into a diffusion chamber. In the diffusion chamber were installed three turbulence screens, Fig. 5. The first screen (1) contained square passages (8×8 mm) parallel to the axis of the diffusion chamber. The length of these passages was 6 cm. The second screen (2) was sheet metal preforated with 8 mm diameter holes. The third screen (3) was a wire screen of 2 mm mesh. Leaving the diffusion chamber the air passed through an accelerating nozzle. The manometer (M_1) was used to select the desired working velocity of the air flow. Attached to the accelerating nozzle was a 100 cm length of 10 cm diameter straight wooden pipe. The test pieces of curved pipe were then installed on the end of this straight pipe.

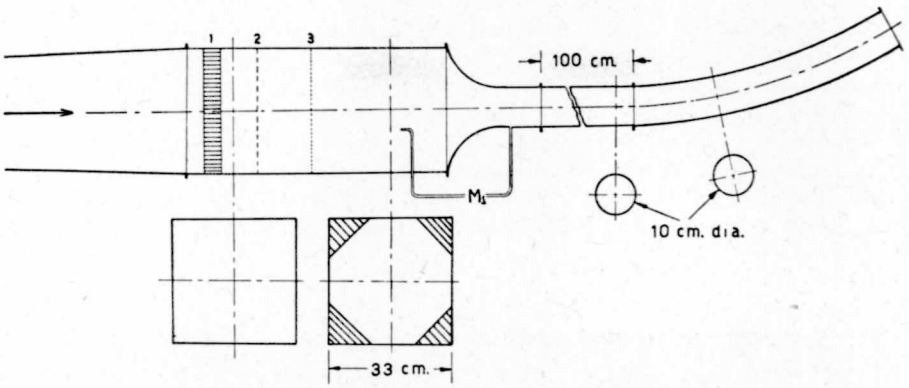

Fig. 5. Schematic sketch of the test apparatus.

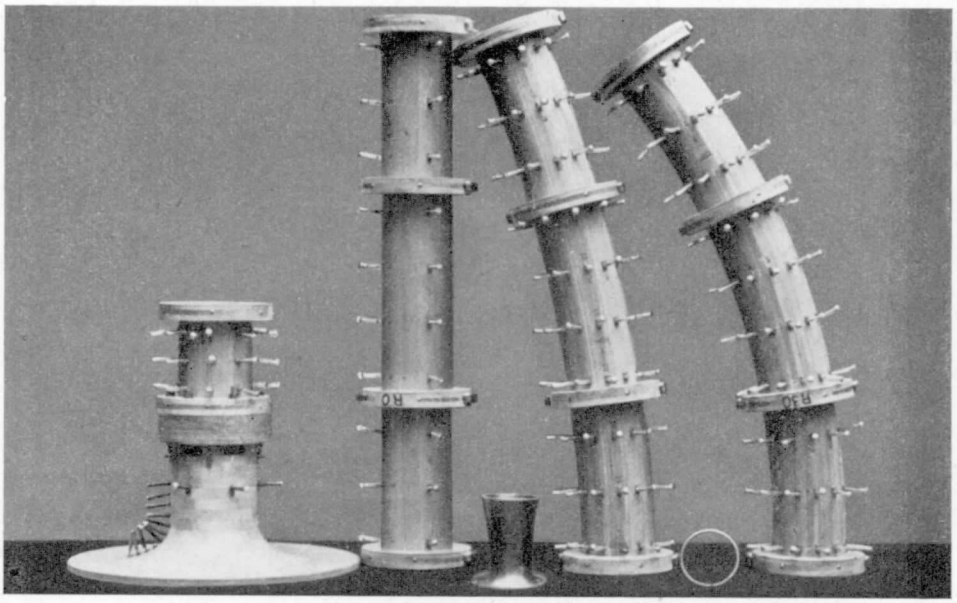

Fig. 6. The accelerating nozzle and wooden pipes used for the experiments.

Because the stagnation pressure distribution at the exit of the accelerating nozzle was very nearly rectangular, the straight section of pipe was used to allow the boundary layer to grow and thus give a slightly pointed distribution. To produce further variations in the stagnation-pressure distribution at the inlet of the curved pipes various combinations of a nozzle-insert and a wire ring, (Fig. 6) installed in the straight pipe were used. The nozzle-insert had a length of 150 mm and a throat diameter of 70 mm. The diameter of the wire used for the ring was 5 mm.

Two wooden curved circular constant-area test pipes were employed for the experiments. Each had a diameter of 10 cm and a length of 100 cm, measured

along the longitudinal axis. Pipe I had a radius of curvature of 273 cm and an angle of bend of 21 degrees. Pipe II had a radius of curvature of 137 cm and corresponding angle of bend of 42 degrees. Both pipes were fitted with 60 pressure taps to measure the wall pressure. The holes in these pressure taps had a diameter of 1 mm. Longitudinally along the pipe six taps were located at each cross-section of the pipe at one diameter intervals, beginning one half of a diameter from the inlet. Within the cross-section the six pressure taps were located at 30 degree intervals starting at $\alpha = 15^\circ$ where $\alpha = 0^\circ$ indicates the inside of the bend.

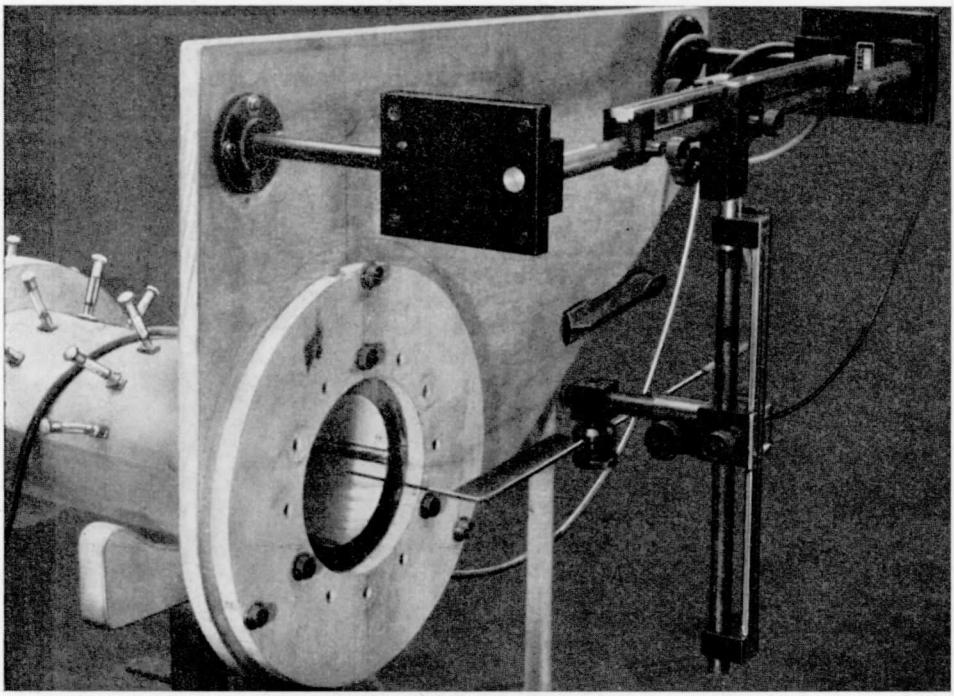

Fig. 7. The arrangement of the compound traverse and the total pressure probe used to measure the total pressure at the exit of the test pipes.

To measure the stagnation-pressure distribution at the exit of the test pipes a total pressure probe, installed on a compound traverse, was used. This probe had an outside diameter of 2,5 mm, an inside of 1 mm and the end was tapered to zero wall thickness. The traverse provided a means of moving the pressure probe in the plane of the exit cross-section of the pipe and at the same time identified the position of the probe. The general arrangement of this traverse is shown in Fig. 7. Assuming that atmospheric static pressure existed at the exit cross-section of the test pipe and with the pressure probe located precisely at the exit of the test pipe, the manometer, vented to atmospheric pressure, indicated directly the dynamic pressure.

§ 3. Test Procedure and Results

A. Test Procedure

Manometer (M_1), measuring the difference between the stagnation pressure in the diffusion chamber and the static pressure in the accelerating nozzle, was used to select a desired average flow velocity based on mass flow. This average mass-flow velocity provided a convenient reference velocity. Nozzle calibration curves were used to determine the manometer reading corresponding to a certain value of average mass-flow velocity. The nozzle calibrations were conducted by Mr. Sprenger of the Institut für Aerodynamik previous to the beginning of the subject experiments.

Using the total pressure probe mounted on the traverse, the stagnation pressure distribution at the exit of the straight section of pipe was first measured with the curved pipe removed. The distribution, so measured, was taken as the inlet stagnation pressure distribution of the curved pipes, which were then attached to this section of straight pipe. Since the measurements were made at the exit of the straight pipe, after the expansion of the flow to atmospheric pressure, the manometer indicated the dynamic pressure at each measured point. The axial velocity was then calculated from this dynamic pressure. The curved test pipe was then installed and using the same value of average mass-flow velocity as used for the above measurements, lines of constant stagnation pressure were measured at the exit of the curved pipe. Here again, since the measurements were made at the exit cross-section after the expansion to atmospheric pressure, the measured pressures indicated the dynamic pressure, from which the axial velocity was calculated. The regions of high stagnation pressure which form in the cross-section toward the outside of the bend then appeared at the exit of the curved pipe as regions of high axial velocity. The difference in the shape of the stagnation pressure distribution at the inlet and exit of a curved pipe, as measured above, shows the effect of the bend with the static pressure eliminated, since both distributions are measured with respect to the same static pressure throughout the cross-section.

B. Experimental Results

Tests were conducted on pipes I and II using four different inlet stagnation pressure distributions. These inlet distributions are denoted by the letters A, B, C, and D. The exit axial-velocity distributions resulting from using these inlet distributions in the test pipes appear respectively in Figs. 8, 9, 10, and 11. The curves plotted are lines of constant axial-velocity ratio $w/\overline{w}$. The $\overline{w}$ indicates the average mass-flow velocity and w is the local axial velocity. The average velocity in the accelerating nozzle and the nozzle diameter were used to define the Reynolds number.

In Fig. 8 are shown the results of tests on pipe I using the approximately rectangular inlet distribution A. This is the distribution as measured at the exit of the accelerating nozzle. For this test the 100 cm length of straight pipe was not used. Here the displacement of the particles with the higher stagnation pressure toward the outside of the bend is evident, however it is relatively small. From a first glance, one might conclude that the deductions made in Chapter I about the effects of the secondary flow are false. In the higher

velocity region, the lines of constant axial velocity show no symmetry or regular form. If the secondary flow does arise from a total pressure gradient, then in this case the contributions come only from a small region close to the wall. Since this region is small, a small non-symmetry of the entrance distribution can show an amplified effect in causing a non-symmetrical secondary

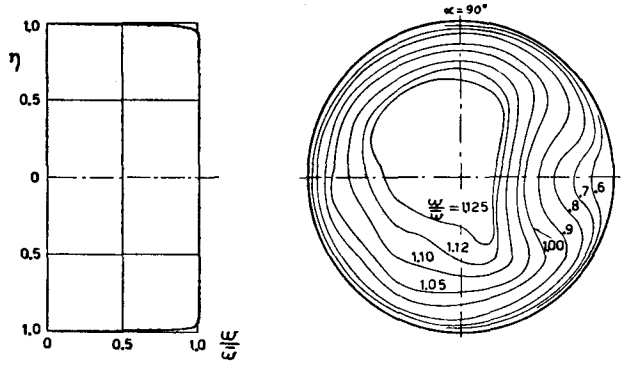

(a) (b)

Fig. 8. Measured lines of constant axial velocity at the exit of: (b), pipe I, with an angle of bend of 21 degrees, resulting from (a), the inlet distribution A, where $\overline{w} = 4150$ cm/sec. and $R_e = 258\,600$.

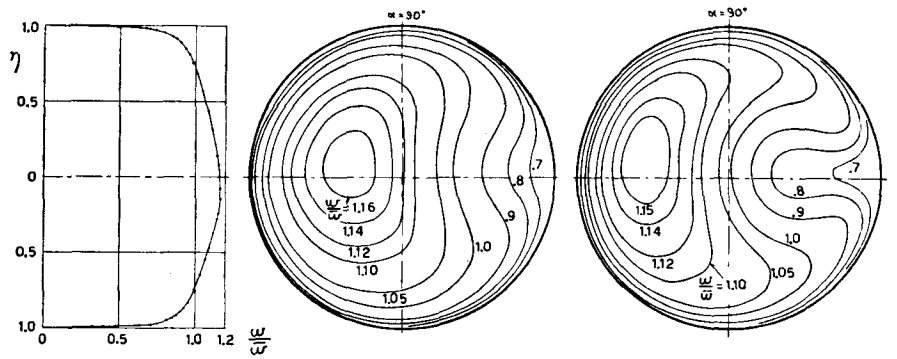

(a) (b) (c)

Fig. 9. Measured lines of constant axial velocity at the exit of: (b), pipe I, with an angle of bend of 21 degrees, and (c), pipe II, with a bend angle of 42 degrees, resulting from (a), inlet distribution B, where $\overline{w} = 4160$ cm/sec. and $R_e = 256\,000$.

flow. Hence, due both to the non-symmetrical inlet distribution and the non-symmetrical secondary flow, it is doubtful that the axial velocity after a bend will show any symmetry. However, the curves in the lower stagnation-pressure region do exhibit a symmetrical shape. Also evident is an increase in velocity of the fluid in the central region of the pipe. Because of a growth of the boundary layer thickness, the effective cross-sectional area of the pipe is decreased, necessitating an acceleration of the fluid in the region outside of the boundary layer in order to satisfy the continuity conditions.

Fig. 9 shows the results of tests on pipes I and II using inlet distribution B, a slightly pointed distribution. This is the distribution measured at the exit of the 100 cm long straight pipe with the wire ring inserted 95 cm from the exit. In the figures showing the measured exit axial-velocity distribution the effect of the secondary flow is quite evident. The particles with the higher stagnation pressure have clearly been displaced toward the outside of the bend. The curves of constant axial velocity exhibit, in general, a symmetrical characteristic indicating the secondary flow was approximately symmetrical. From the results of pipe II, corresponding to a 42 degree bend, it is clear that the displacement of the higher stagnation-pressure particles toward the outside of the bend has forced the particles with the lower stagnation pressure to move along the wall of the pipe toward the inside of the bend. As a result of this motion, clearly defined regions of low stagnation-pressure fluid are located at the inside of the bend.

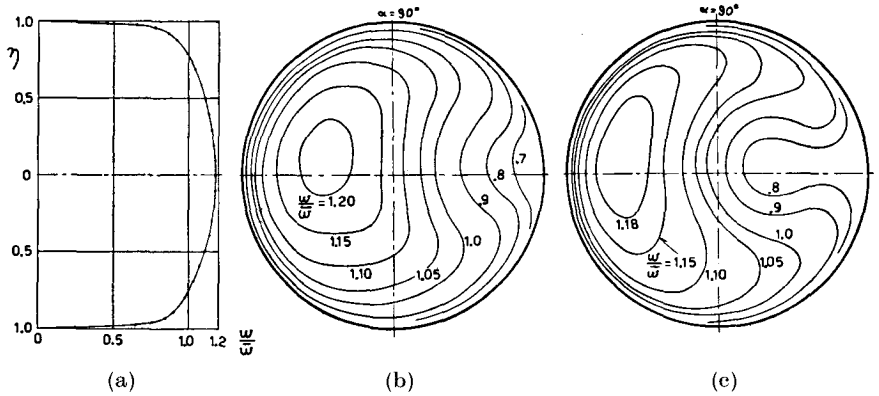

(a) (b) (c)

Fig. 10. Measured lines of constant axial velocity at the exit of: (b), pipe I, with an angle of bend of 21 degrees, and (c), pipe II, with a bend angle of 42 degrees, resulting from (a), inlet distribution C, where $\overline{w} = 4200$ cm/sec. and $R_e = 250000$.

The results of tests on pipes I and II using the distribution C, which is only slightly different from B, are shown in Fig. 10. This distribution was obtained by installing the nozzle-insert in the short constant-area section of the accelerating nozzle. The distribution was then measured at the exit of the 100 cm length of straight pipe. The results show the same general character as those using distribution B. The displacement of the higher stagnation-pressure fluid particles toward the outside of the bend is slightly larger than the case above. The entrance distribution C, however, has a slightly larger velocity variation than distribution B. This then indicates that the effect of the secondary flow increases as the stagnation-pressure gradient increases. The regions of low velocity fluid at the inside of the bend of pipe II are well defined and are showing a tendency to become closed regions.

The results of tests using pipes I and II and a more pointed inlet distribution D, are given in Fig. 11. These results, displaying the same tendencies as those above, also confirm the deductions made in Chapter I about the effect of the secondary flow on the stagnation-pressure distribution. The rather sharply pointed characteristic of the inlet distribution has been to some extent

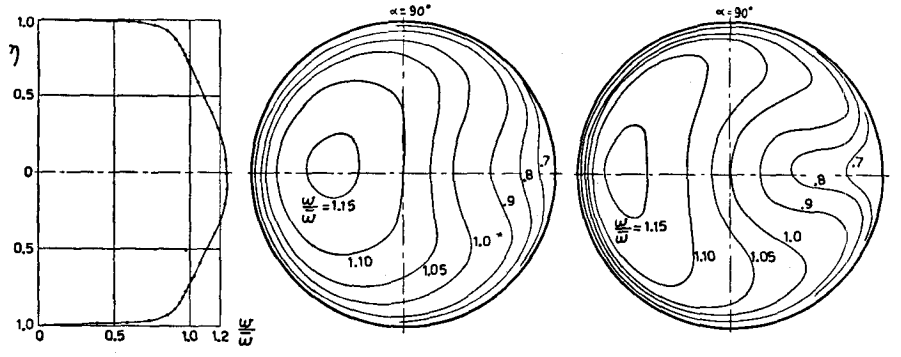

(a) (b) (c)

Fig. 11. Measured lines of constant axial velocity at the exit of: (b), pipe I, with an angle of bend of 21 degrees, and (c), pipe II, with a bend angle of 42 degrees, resulting from (a), inlet distribution D, where $\bar{w} = 4180$ cm/sec. and $R_e = 252000$.

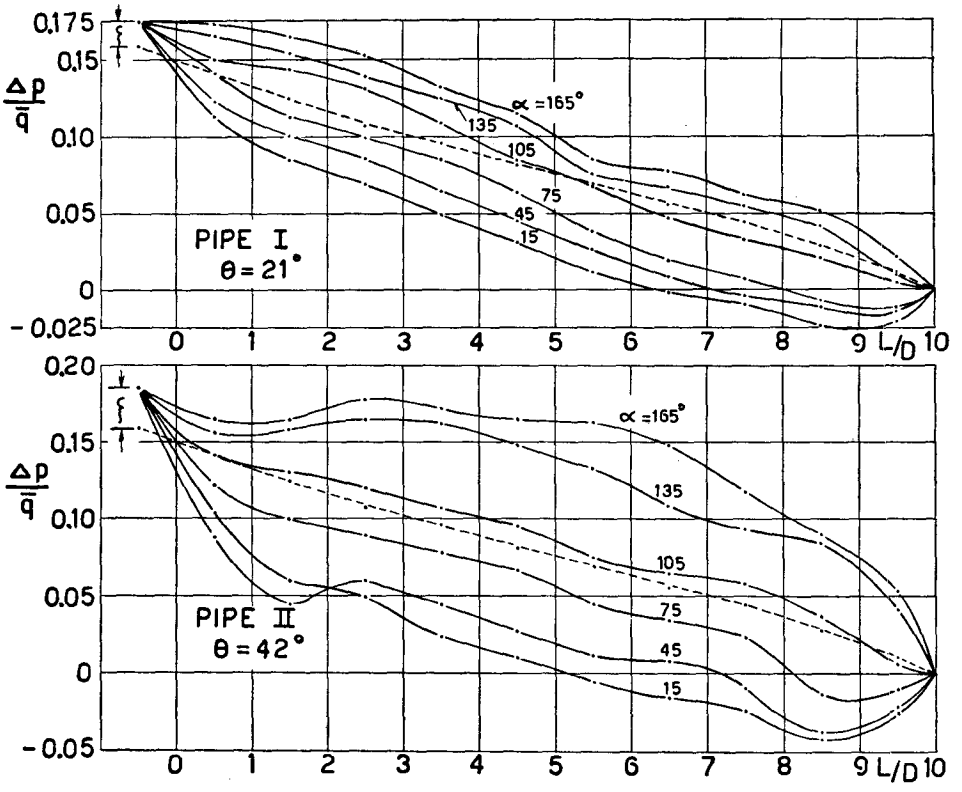

Fig. 12. Wall static pressure variation along curved pipes I and II, resulting from inlet distribution B. $\alpha = 0 =$ inside of bend. $\bar{q} = 9789$ dyn/cm^2.

flattened as the fluid moved around the bend. This is the result of the usual characteristics of a pointed velocity distribution, at high Reynolds numbers, to transform into the customary turbulent velocity distribution.

The wall static pressure variations for pipes I and II, which resulted from using distribution B, are shown in Fig. 12. The distance along the length of the pipe, plotted as the abscissa, is measured by the number of diameters downstream from the entrance. The ordinate is the dimensionless difference between the wall static pressure and atmospheric pressure. The angles noted on each curve denote the location of the pressure tap on the circumference of the cross-section, where $\alpha = 0°$ is on the inside of the bend.

The curves show the usual expansion to atmospheric pressure, however there is evident a difference in the circumferential wall static pressure at any one cross-section. This then indicates the effect of the bend in the respect that there is a deviation from the single straight line which would occur for a straight pipe. A comparison between the results from pipe I and II shows that as the angle of bend increases the spread in the curves of the pressure on the inside and outside of the bend also increases. From this we can see the transition from a straight pipe to a curved pipe. A straight pipe would yield only one curve and as the pipe is slightly bent the curves would separate a small amount, this separation then increasing as the bend in the pipe is increased. The wall pressures on the outside of the bend remain above atmospheric pressure during the expansion while those on the inside of the bend reduce below atmospheric pressure. If the flow entered the curve as potential flow the higher velocity on the inside of the bend would first cause a decrease in the wall pressure while the lower velocity on the outside of the bend would cause an increase in the wall pressure. In the bend the fluid particles would tend toward the inside of the bend and then under the action of the centrifugal force this concentration of high velocity fluid on the inside of the bend would be forced to move toward the outside of the bend causing a further decrease in the pressure on the inside of the bend and an increase on the outside of the bend. In the plotted curves the effect of the flow in the bend on the wall static pressure is coupled with the expansion to atmospheric pressure.

For comparision, the pressure drop in the straight pipe is also plotted (dashed curve). The static pressure drop due to the bend losses, indicated by the ordinate difference at one half of a diameter upstream of the entrance to the curved pipes, are $0.016\,\bar{q}$ for pipe I, corresponding to a bend angle of 21 degrees, and $0.027\,\bar{q}$ for pipe II, corresponding a 42 degree bend angle.

Chapter IV. Theory for the Secondary Flow in Curved Pipes

§ 1. The General Problem

As was seen from the experimental results, which support the physical conjectures already made, a secondary flow phenomenon does arise when a fluid, with a non-uniform inlet stagnation-pressure distribution, flows in a curved pipe. The effect of this phenomenon is to displace the fluid particles with the higher stagnation pressure toward the outside of the bend and at the same time cause a region of low stagnation pressure fluid to form on the inside of

the bend. The problem is then to formulate this secondary flow and its subsequent effect on the principal flow, through an application of the equations of motion.

In reality, the solution of this problem should be obtained from a solution of the complete Navier-Stokes equations of motion, in which the viscosity as well as the inertia effects are brought into consideration. However, the solution of these equations for the general case remains one of the classical unsolved problems. To be sure, the Navier-Stokes equations can be solved exactly for a few very special cases, but unfortunately the problem at hand does not lie within this catagory of simplification. In the following analysis all of the viscous effects will be neglected and therefore the viscous terms in the Navier-Stokes equations will be omitted. Under these conditions, i.e. the assumption of an inviscid fluid, the problem is reduced to the study of the flow of an "ideal" fluid. In addition, only the steady-state incompressible phenomenon will be investigated.

Into this study of an "ideal" fluid flow we wish to introduce the fact that the stagnation-pressure at the inlet of the curved pipe is non-uniform. From the physical arguments of Chapter I it would be expected that no secondary flow arises from a uniformly-constant inlet-stagnation-pressure distribution. These non-uniform distributions, to be considered, must however satisfy certain conditions. In particular, they are required to have finite non-zero velocities along the wall of the pipe. Suppose, for example, that the velocity is taken as zero on the boundary. Then to apply the theory to a fully developed turbulent flow, it would be necessary to have a very large velocity gradient in the region close to the wall of the pipe. We know, however, from the results of the theory of fluids of small (but not zero) viscosity, that the shearing stress in a viscous fluid is proportional to the velocity derivatives. So under these circumstances of large velocity gradients, the inviscid-fluid approximations no longer apply and it is necessary to retain the viscous terms in the equations of motion. On the other hand, it is known that the "ideal" fluid flow results give a good approximation to the actual outside of the boundary-layer and other regions of large velocity gradients. So the assumption of a finite velocity on the pipe wall is in accordance with the "ideal" fluid approximations.

The general steady-state Eulerian partial differential equations of motion for any frictionless fluid are

$$\rho u_k \frac{\partial u_i}{\partial x_k} = -\frac{\partial p}{\partial x_i} + \rho f_i \qquad i, k = 1, 2, 3.$$

where

u = velocity component
p = pressure
ρ = mass density
f = body force per unit mass.

The flow must also satisfy the continuity equation which reads, for an incompressible fluid

$$\frac{\partial u_k}{\partial x_k} = 0.$$

To apply these equations to the problem of flow in a curved pipe, they must of course be expanded in terms of appropriate coordinates. We choose the

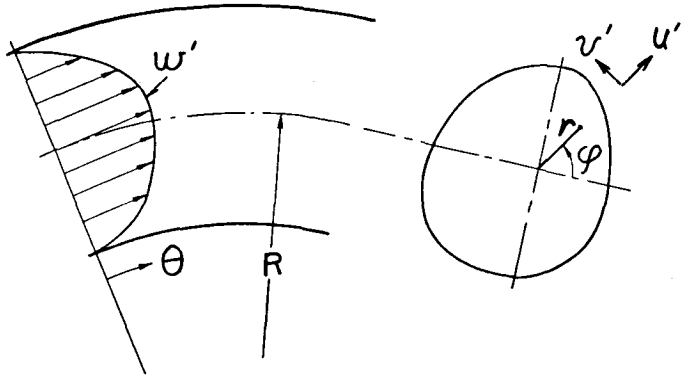

Fig. 13. The coordinate system for the general problem.

coordinate system indicated in Fig. 13, with the radius of curvature assumed to be constant. The line element in terms of these coordinates becomes

$$(ds)^2 = (dr)^2 + r^2(d\varphi)^2 + (R + r\sin\varphi)^2(d\theta)^2.$$

Expanding the equations of motion in terms of the velocity components and coordinates as indicated and with $f_i = 0$, we obtain the following system of equations ([16] gives the equations of motion in general orthogonal coordinates).

$$u'\frac{\partial u'}{\partial r} + \frac{v'}{r}\frac{\partial u'}{\partial \varphi} + \frac{w'}{R + r\sin\varphi}\frac{\partial u'}{\partial \theta} - \frac{v'^2}{r} - \frac{w'^2\sin\varphi}{R + r\sin\varphi} = -\frac{1}{\rho}\frac{\partial p'}{\partial r} \tag{8a}$$

$$u'\frac{\partial v'}{\partial r} + \frac{v'}{r}\frac{\partial v'}{\partial \varphi} + \frac{w'}{R + r\sin\varphi}\frac{\partial v'}{\partial \theta} + \frac{u'v'}{r} - \frac{w'^2\cos\varphi}{R + r\sin\varphi} = -\frac{1}{\rho}\frac{1}{r}\frac{\partial p'}{\partial \varphi} \tag{8b}$$

$$u'\frac{\partial w'}{\partial r} + \frac{v'}{r}\frac{\partial w'}{\partial \varphi} + \frac{w'}{R + r\sin\varphi}\frac{\partial w'}{\partial \theta} + \frac{w'}{R + r\sin\varphi}(u'\sin\varphi + v'\cos\varphi) = -\frac{1}{\rho}\frac{1}{R + r\sin\varphi}\frac{\partial p'}{\partial \theta} \tag{8c}$$

$$\frac{\partial}{\partial r}(ru') + \frac{\partial v'}{\partial \varphi} + \frac{r}{R + r\sin\varphi}\frac{\partial w'}{\partial \theta} + \frac{r}{R + r\sin\varphi}(u'\sin\varphi + v'\cos\varphi) = 0. \tag{8d}$$

The velocities in the above equations represent the total values, that is the initial value plus any variation, so that the equations are non-linear. The system, with four equations and four dependent unknowns, is sufficient for eliminating three of the unknowns to obtain one equation with one unknown. Unfortunatly, there is little hope of solving the resulting non-linear partial differential equation of at least the fourth order. Consequently, a new method of approach to the problem will be applied, one whose solution can readily be found.

§ 2. A New Approach and its Solution for Circular Pipes

We consider here a circular pipe of constant cross-sectional area. Let us say that the pipe remains straight and that each fluid particle is acted upon by a body force, acting in the plane perpendicular to the longitudinal axis of the pipe. The magnitude of this body force is taken to be a constant times the

square of the particle's axial velocity. We choose this constant such that the body force corresponds to the centrifugal force which would be present for a particular bent pipe. That is to say, the constant is equal to the reciprocal of the radius of curvature of the path of the fluid particle flowing in this bent pipe.

Under these considerations, the equations of motion can be written in terms of cylindrical coordinates as

$$u'\frac{\partial u'}{\partial r}+\frac{v'}{r}\frac{\partial u'}{\partial \varphi}+w'\frac{\partial u'}{\partial z}-\frac{v'^2}{r}=-\frac{1}{\rho}\frac{\partial p'}{\partial r}+f_r \tag{9a}$$

$$u'\frac{\partial v'}{\partial r}+\frac{v'}{r}\frac{\partial v'}{\partial \varphi}+w'\frac{\partial v'}{\partial z}+\frac{u'v'}{r}=-\frac{1}{\rho}\frac{1}{r}\frac{\partial p'}{\partial \varphi}+f_\varphi \tag{9b}$$

$$u'\frac{\partial w'}{\partial r}+\frac{v'}{r}\frac{\partial w'}{\partial \varphi}+w'\frac{\partial w'}{\partial z}=-\frac{1}{\rho}\frac{\partial p'}{\partial z}, \tag{9c}$$

and the continuity equation becomes

$$\frac{\partial}{\partial r}(r\,u')+\frac{\partial v'}{\partial \varphi}+r\frac{\partial w'}{\partial z}=0. \tag{9d}$$

The coordinate system and the direction of the velocity components are shown in Fig. 14. The body force f is zero for $z<0$.

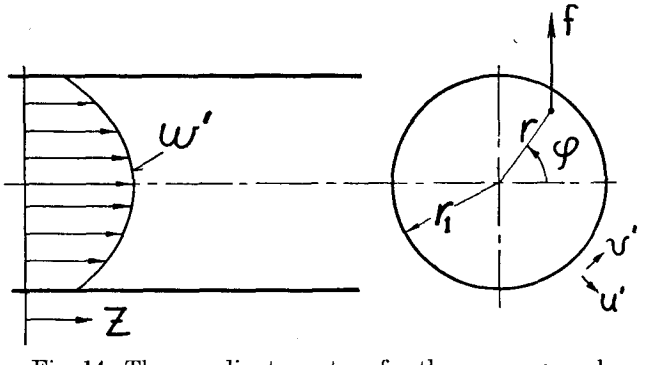

Fig. 14. The coordinate system for the new approach.

As we have seen from the experimental wall pressure distributions along the length of the curved pipes, the spread of the curves representing the wall pressure at the different circumferential locations of the cross-section decreases as the angle of bend decreases. For small bend angles the spread of these curves should likewise be small, for in the limiting case of no bend they merge into one single straight line. This limiting case, as applied to a frictionless fluid flow, corresponds to the case of no pressure drop along the length of the pipe and consequently no change in the longitudinal velocity. For this investigation of the initial phases of the secondary flow, which then corresponds to the study of the flow in a slightly bent pipe, it is assumed that each particle's axial velocity remains constant at its inlet value. To obtain the change of the axial-velocity profile due to the secondary flow, each particle will be displaced from

its inlet position within the cross-section to a new position as required by the secondary flow, but still retaining its initial inlet-axial velocity.

The above equations can be linearized by making the following assumptions. We say that in the inlet flow, i.e. $z \leqq 0$, the secondary flow does not exist. The secondary flow velocities are assumed to grow, but not rapidly, as the flow moves beyond the section $z = 0$. Then the secondary velocity components u' and v' can be considered small compared to the inlet velocity w'. If the velocities u' and v' are small in comparison to the axial velocity, the secondary flow can be considered as a perturbation superimposed on the principal flow. From continuity it follows that the derivatives of the secondary velocities are of the same order of magnitude as the secondary velocities themselves and can be handled accordingly. The validity of the perturbation approximations requires that the correction on the principal flow always be small. We notice here, that if the case of an inlet stagnation pressure distribution with zero velocity on the wall of the pipe were considered, the secondary flow velocities in the region close to the wall could be of the same order of magnitude as the axial velocity. Under these circumstances the above assumption would certainly break down near the wall of the pipe. Using this assumption in the equations of motion, all terms containing products, squares or higher powers of the secondary flow quantities can be neglected.

With the small perturbation approximation and with the assumption of no change in the value of the axial velocity, the total velocity components and pressure, which appear in (9), can be written as follows:

$$u' = 0 + u \qquad w' = w$$
$$v' = 0 + v \qquad p' = p_0 + p$$

Substituting these relations into (9) and neglecting the higher order terms, we obtain the following system of equations.

$$w \frac{\partial u}{\partial z} = -\frac{1}{\rho} \frac{\partial p}{\partial r} + f_r \tag{10}$$

$$w \frac{\partial v}{\partial z} = -\frac{1}{\rho} \frac{1}{r} \frac{\partial p}{\partial \varphi} + f_\varphi \tag{11}$$

$$\frac{\partial}{\partial r}(r u) + \frac{\partial v}{\partial \varphi} = 0. \tag{12}$$

With the assumption of no variation of the magnitude of the longitudinal velocity and by considering the secondary flow as a small perturbation on the principal flow, the variation in the static pressure in the cross-section and along the length of the pipe has been essentially eliminated. To be sure, (10) and (11) show that a static pressure variation will arise from the secondary flow, but if the secondary flow is small then this variation in static pressure will also be small. The results of a theory developed under these assumptions will then show the effect of the secondary flow in bends, approximately independent of the variations in the static pressure. Since the results of the experimental investigations are also based on the same static pressure at the entrance and exit cross-section of the curved pipes, this makes a comparison between the theory and the experiments more feasible.

Equation (12) can be integrated immediately by introducing a stream function defined by

$$u = \frac{1}{r}\frac{\partial \psi}{\partial \varphi}; \qquad v = -\frac{\partial \psi}{\partial r}. \tag{13}$$

By putting these definitions into (10) and (11) and after eliminating the perturbation pressure by cross differentiation, the following equation results:

$$\frac{\partial}{\partial \varphi}\left(\frac{w}{r}\frac{\partial^2 \psi}{\partial \varphi\, \partial z}\right) + \frac{\partial}{\partial r}\left(r w \frac{\partial^2 \psi}{\partial r\, \partial z}\right) = \frac{\partial}{\partial \varphi}(f_r) - \frac{\partial}{\partial r}(r f_\varphi).$$

The velocity w is taken as only the inlet velocity and is therefore not a function of z, thus this equation can be integrated with respect to z yielding

$$\frac{\partial}{\partial \varphi}\left(\frac{w}{r}\frac{\partial \psi}{\partial \varphi}\right) + \frac{\partial}{\partial r}\left(r w \frac{\partial \psi}{\partial r}\right) = z\left(\frac{\partial}{\partial \varphi}(f_r) - \frac{\partial}{\partial r}(r f_\varphi)\right) + g(r, \varphi).$$

But at the inlet section, i.e. $z = 0$, we have assumed that the secondary flow is zero, so $u = v = 0$. Therefore $g(r, \varphi) = 0$ and,

$$\frac{\partial}{\partial \varphi}\left(\frac{w}{r}\frac{\partial \psi}{\partial \varphi}\right) + \frac{\partial}{\partial r}\left(r w \frac{\partial \psi}{\partial r}\right) = z\left[\frac{\partial}{\partial \varphi}(f_r) - \frac{\partial}{\partial r}(r f_\varphi)\right]. \tag{14}$$

From our previous discussion about the body force f, we require its components to be

$$f_r = \frac{w^2}{R\left(1 + \frac{r}{R}\sin\varphi\right)}\sin\varphi; \qquad f_\varphi = \frac{w^2}{R\left(1 + \frac{r}{R}\sin\varphi\right)}\cos\varphi,$$

where $R\left(1 + \frac{r}{R}\sin\varphi\right)$ is the radius of curvature of the path of the particle. Since we are considering only curved pipes whose ratio of radius to radius of curvature is much less than one

$$R\left[1 + \max.\left(\frac{r}{R}\sin\varphi\right)\right] = R\left[1 + \frac{r_1}{R}\right] \approx R.$$

Having now evaluated the body force we can see the transition from the general case of § 1 to this new approach. A comparison of the terms of equations (8, 9a, b) shows the body force, as used here, also appears in (8a, b). The simplification of equations (9c, d) as compared to (8c, d) results from the differences in the coordinate systems.

Introducing the body force as approximated above into (14) leads to

$$\frac{\partial^2 \psi}{\partial r^2} + \left(\frac{1}{r} + \frac{1}{w}\frac{\partial w}{\partial r}\right)\frac{\partial \psi}{\partial r} + \frac{1}{r^2 w}\frac{\partial w}{\partial \varphi}\frac{\partial \psi}{\partial \varphi} + \frac{1}{r^2}\frac{\partial^2 \psi}{\partial \varphi^2} = \frac{2z}{R}\left[\frac{1}{r}\frac{\partial w}{\partial \varphi}\sin\varphi - \frac{\partial w}{\partial r}\cos\varphi\right]. \tag{15}$$

The stream function satifying (15) will yield the desired solution for the secondary flow. For a given problem with $\omega(r, \varphi)$ a known function, the solution can be obtained numerically by the methods of relaxation of other numerical methods. However further simplifications result if the inlet-velocity distribution is assumed to be symmetrical about the longitudinal axis, that is $\omega = \omega(r)$ only. Clearly, this assumption has obvious mathematical advantages

and is not greatly restrictive in the practical sense, since in many applications the actual velocity distribution can be approximated closely as being symmetrical. Under these circumstances (15) reduces to

$$\frac{\partial^2 \psi}{\partial r^2} + \left(\frac{1}{r} + \frac{1}{w}\frac{dw}{dr}\right)\frac{\partial \psi}{\partial r} + \frac{1}{r^2}\frac{\partial^2 \psi}{\partial \varphi^2} = -\frac{2z}{R}\frac{dw}{dr}\cos\varphi. \tag{16}$$

We see immediately that this partial differential equation can be reduced to an ordinary differential equation by making the substitution of the form

$$\psi \sim \sigma(r)\cos\varphi.$$

The form of this stream function is recognized as the same as the stream function predicted in Chapter II. Thus the streamlines will have the same general shape as those obtained there. At the same time we introduce the following dimensionless parameters:

$$\eta = \frac{r}{r_1}, \quad \text{where } r_1 = \text{outside radius of the pipe}$$

$$\beta = \frac{w}{w_0}, \quad \text{where } w_0 = \text{maximum value of the inlet velocity}$$

$$\frac{z}{r_1} = \delta$$

$$\frac{r_1}{R} = \lambda, \quad \text{thus } \theta = \lambda\delta, \text{ the bend angle.}$$

$$\sigma(\eta)\cos\varphi = \frac{\psi}{\lambda\delta r_1 w_0}.$$

Upon substitution of the above relations into (16), we arrive at the following ordinary differential equation

$$\frac{d^2\sigma}{d\eta^2} + \left(\frac{1}{\eta} + \frac{1}{\beta}\frac{d\beta}{d\eta}\right)\frac{d\sigma}{d\eta} - \frac{\sigma}{\eta^2} = -\frac{2\,d\beta}{d\eta}. \tag{17}$$

The boundary conditions to be satisfied by $\sigma(\eta)$, the solution of (17), are

$$\sigma(1) = 0; \quad \sigma(0) = 0.$$

The first boundary condition comes simply from the requirement that there be no flow through the wall of the pipe, that is the wall of the pipe must be a streamline. We justify the second boundary condition with the following argument. Since the independent variable φ was eliminated from the differential equation by the substitution of $\cos\varphi$, the resulting streamlines of the secondary flow will be symmetrical about a line through the center of the pipe and parallel to the body force f. Now along the line $\varphi = 0$ and in the immediate vicinity of $\eta = 0$ the flow must appear approximately as parallel flow. Thus for very small values of η the function $\sigma(\eta)$ must have the form $\sigma(\eta) \sim \eta$. Consequently, for $\eta = 0$ the function $\sigma(\eta)$ must also be zero.

A solution of (17) can be obtained by series integration. The singularity of the differential equation at $\eta = 0$ is non-essential, so that according to Fuchs theorem a convergent development of the solution in a power series about the singular point is possible. The details of this method are presented in [17]. The

differential equation does not admit a solution in terms of known functions such as hyper-geometric or Bessel functions. We therefore elect to find an approximate solution of (17) in the form of the finite series

$$\sigma(\eta) = \sum_{k=1}^{n} a_k \eta^k . \tag{18}$$

Upon substituting this assumed solution into (17) and collecting terms we obtain

$$\sum_{k=1}^{n} (k^2 - 1) a_k \eta^{k-2} + \frac{1}{\beta} \frac{d\beta}{d\eta} \sum_{1}^{n} k a_k \eta^{k-1} = -2 \frac{d\beta}{d\eta}. \tag{19}$$

Since the function $\beta(\eta)$ is known throughout the interval $0 \leqq \eta \leqq 1$, we can evaluate (19) in any selected number of points and thereby obtain a system of algebraic equations for the determination of the coefficients a_k. For example, if we wish to satisfy (19) at, say, j points, then in the solution we will have $k = j + 1$. With (19) satisfied at j points, and along with (18) evaluated at $\eta = 1$, that is

$$\sigma(1) = \sum_{1}^{n} a_k = 0 ,$$

we obtain $j + 1$ algebraic equations. The simultaneous solution of these equations yields the $j + 1$ constant coefficients. Obviously, as j increases the solution more closely approximates the exact solution. An example showing the convergence characteristics of this method of solution is given in Appendix A.

Upon inspection of (19) when expanded for the value $\eta = 0$, we find that $a_2 = 0$ if $\left(\frac{d\beta}{d\eta}\right)_{\eta=0} = 0$. Since we have already assumed symmetry for the inlet-velocity distribution, this simply requires that β be a smooth function as it passes through the point $\eta = 0$. Cases where this is not true are only of academic interest. Thus, in the summations of (19) the value $k = 2$ can be omitted.

By using the above method, a solution for the secondary stream function can be obtained as

$$\psi = \lambda \delta r_1 w_0 \sum_{1}^{n} a_k \eta^k \cos\varphi , \tag{20}$$

from which the secondary velocities are given by

$$\begin{aligned} u &= -\lambda \delta w_0 \sum_{1}^{n} a_k \eta^{k-1} \sin\varphi \\ v &= -\lambda \delta w_0 \sum_{1}^{n} k a_k \eta^{k-1} \cos\varphi . \end{aligned} \tag{21}$$

We now superimpose these secondary velocities on the principal flow to investigate their effect on changing the shape of the axial-velocity distribution. Since it was already assumed that each fluid particle's axial velocity remains constant, we fix our attention on a given particle and observe its motion under the influence of the secondary flow. The differential equations for determining the path of a particle are

$$\frac{dr}{dz} = \frac{u}{w} ; \qquad \frac{r\,d\varphi}{dz} = \frac{v}{w} ,$$

or upon substituting the values of u and v from (21), these become

$$d\eta = -\frac{\lambda}{\beta}\sum_{1}^{n} a_k \eta^{k-1} \sin\varphi\, \delta\, d\delta$$

and

$$d\varphi = -\frac{\lambda}{\beta}\sum_{1}^{n} k\, a_k \eta^{k-2} \cos\varphi\, \delta\, d\delta\,.$$

The above equations are solved as follows

$$\begin{aligned} \Delta\eta &= \eta_2 - \eta_1 = -\frac{\lambda(\delta_2{}^2 - \delta_1{}^2)}{2\beta}\left[\sum_{1}^{n} a_k \eta^{k-1}\right]_A \sin\varphi_A \\ \Delta\varphi &= \varphi_2 - \varphi_1 = -\frac{\lambda(\delta_2{}^2 - \delta_1{}^2)}{2\beta}\left[\sum_{1}^{n} k\, a_k \eta^{k-1}\right]_A \cos\varphi_A\,, \end{aligned} \tag{22}$$

where the subscript A indicates the average value between the cross-sections 1 and 2 is to be taken. The accuracy of these average values can be increased by iteration. To use these equations we simply select a definite particle at the entrance and calculate its path as defined by $\Delta\eta$ and $\Delta\varphi$ as it moves around the bend. This then requires a step-wise computation from one cross-section to the next, proceeding around the bend. The accuracy of these calculations is increased as the interval between the stations 1 and 2 is decreased.

The secondary flow stream function obtained from (17) is dependent on the inlet-velocity distribution. This same stream function is then used at all stations downstream of the inlet. Clearly, the secondary flow is a function of the local axial-velocity distribution. Hence, it would be necessary to solve anew for the secondary flow velocities at each cross-section where (22) are applied, using the local axial-velocity distribution. In view of the approximations already made, this refinement is of problematic value.

As discussed previously, the secondary flow in the plane of the cross-section of the pipe contains vorticity. In particular there will be a definite distribution of vorticity within the cross-section as determined by the gradients of the secondary flow velocities. From the definition of the vector vorticity, i.e. the curl of the velocity vector, the axial component representing the vorticity in the plane of the cross-section of the pipe is given by

$$\gamma(r,\varphi) = \frac{1}{r}\frac{\partial}{\partial r}(r\,v) - \frac{1}{r}\frac{\partial u}{\partial\varphi}.$$

Using the secondary flow velocities (21) as obtained in the above analysis, this vorticity is given by

$$\gamma(\eta,\varphi) = -\frac{\theta\, w_0}{r_1}\sum_{1}^{n}(k^2-1)\, a_k \eta^k \cos\varphi\,.$$

Thus we see the vorticity distribution is symmetrical about a line perpendicular to the plane of the bend of the pipe and exhibits a functional dependence on the radius of the pipe. This functional dependence on the radius is determined in part by the inlet-velocity distribution, since the constant coefficients a_k are determined from the solution of (17), in which the inlet-velocity distribution shows a strong influence.

§ 3. The Relation between the Vorticity and the Axial Velocity

An interesting extension of the theory can be made to show the relation between the vorticity and the axial velocity by using the results of Chapter II and the simplified equations of motion of the last section.

The polar velocity components (3i) and (4b), due to a distribution of vortices over a plane bounded circular area, satisfy uniquely the continuity equation (12). So by considering the velocities (3i) and (4b) as the small perturbation velocities of the secondary flow, we have along with (10) and (11) a system of four equations and four unknowns. The unknowns here are the preturbation velocities u and v, the perturbation pressure p and the vorticity γ, which appears as a function of the radius only.

Using once again the assumptions that the axial velocity w does not vary along the length of the pipe, and that at the inlet it is symmetrical about the longitudinal axis, equations (10) and (11) become after elimination of the pressure and integration with respect to z:

$$\left[\frac{1}{r}\frac{\partial}{\partial r}(r\,v)-\frac{1}{r}\frac{\partial u}{\partial \varphi}\right]+\frac{v}{w}\frac{dw}{dr}=-\frac{z}{w\,r}\left[\frac{\partial}{\partial \varphi}(f_r)-\frac{\partial}{\partial r}(r\,f_\varphi)\right].$$

We recognize the first term in this equation as the vorticity in the plane of the cross-section of the pipe. So by writing the vorticity as $\gamma(r,\varphi)=h(r)\cos\varphi$ and introducing the body force components, as evaluated for a circular pipe in § 2, the above equation reduces to

$$h(r)\cos\varphi+\frac{v}{w}\frac{dw}{dr}=\frac{2z}{R}\frac{dw}{dr}\cos\varphi.$$

The tangential secondary flow velocity component can be eliminated by using (4b), and there results the following integral equation

$$h(r)=2\,\theta\frac{dw}{dr}-\frac{1}{2w}\frac{dw}{dr}\left\{\frac{1}{r^2}\int_0^r\rho^2 h(\rho)\,d\rho+\frac{1}{r_1^{\,2}}\int_0^{r_1}\rho^2 h(\rho)\,d\rho-\int_r^{r_1}h(\rho)\,d\rho\right\}.$$

The above integral equation shows the relation between the vorticity and the inlet-axial velocity, in that the vorticity is equal to twice the angular displacement of the fluid multiplied by the first derivative of the inlet velocity minus a term in which the vorticity and the inlet velocity are coupled. *Squire* and *Winter* [10] found for curved flow in a passage bounded by two circular arcs, where the complete basic motion is represented approximately by uniform approach flow and with uniform flow downstream of the bend, that the axial vorticity in the exit stream is equal to the velocity gradient in the approaching stream multiplied by twice the angular displacement.

For a given inlet-velocity distribution the solution of the above integral equation will yield the corresponding axial vorticity $\gamma(r,\varphi)$ in a bent circular pipe. From the other point of view, the reverse problem of finding the inlet velocity which produces a given vorticity distribution can also be solved with this equation. In this case, if the vorticity is known or assumed, the integrals can be immediately evaluated and hence the integral equation is reduced to an ordinary differential equation. In the practical sense, however, the inlet velocity is known and it is from this known condition that the secondary flow problem must be solved.

§ 4. The Theory for Elliptic Pipes

In this analysis we follow the same approach as used in the last section, in that it is assumed that the pipe remains straight and each fluid particle is acted upon by a body force which is a function of the particle's axial velocity. Under this assumption elliptic cylindrical coordinates can be introduced which are defined by:

$$x = c\cosh\xi\cos\varphi;\quad y = c\sinh\xi\sin\varphi;\quad z = z.$$

For these coordinates the line element is given by:

$$(ds)^2 = c^2(\sinh^2\xi + \sin^2\varphi)(d\xi)^2 + c^2(\sinh^2\xi + \sin^2\varphi)(d\varphi)^2 + dz^2.$$

The foci of the confocal ellipses and hyperbolas are located at $x = \pm c$. If now we let a given value of ξ, say ξ_0, define an entire ellipse, then the limits of the variables ξ and φ must correspond to:

$$0 \leqq \xi \leqq \infty$$
$$0 \leqq \varphi \leqq 2\pi.$$

Let us say the ellipse defining the boundary of the pipe is given by $\xi = \xi_0$. The semi-major and -minor axes then become

$$a = c\cosh\xi_0$$
$$b = c\sinh\xi_0,$$

from which

$$\xi_0 = \frac{1}{2}\ln\frac{a+b}{a-b};\qquad c = \sqrt{a^2-b^2}.$$

The Eulerian differential equations of motion in these coordinates become

$$\frac{u'}{cG}\frac{\partial u'}{\partial\xi} + \frac{v'}{cG}\frac{\partial u'}{\partial\varphi} + w'\frac{\partial u'}{\partial z} + \frac{u'v'}{c^2G^2}\frac{\partial}{\partial\varphi}(cG) - \frac{v'^2}{c^2G^2}\frac{\partial}{\partial\xi}(cG) = -\frac{1}{\rho}\frac{1}{cG}\frac{\partial p'}{\partial\xi} + F_\xi$$

$$\frac{u'}{cG}\frac{\partial v'}{\partial\xi} + \frac{v'}{cG}\frac{\partial v'}{\partial\varphi} + w'\frac{\partial v'}{\partial z} + \frac{u'v'}{c^2G^2}\frac{\partial}{\partial\xi}(cG) - \frac{u'^2}{c^2G^2}\frac{\partial}{\partial\varphi}(cG) = -\frac{1}{\rho}\frac{1}{cG}\frac{\partial p'}{\partial\varphi} + F_\varphi$$

$$\frac{u'}{cG}\frac{\partial w'}{\partial\xi} + \frac{v'}{cG}\frac{\partial w'}{\partial\varphi} + w'\frac{\partial w'}{\partial z} = -\frac{1}{\rho}\frac{\partial p'}{\partial z},$$

and the continuity equation is

$$\frac{\partial}{\partial\xi}(Gu') + \frac{\partial}{\partial\varphi}(Gv') + c\frac{\partial}{\partial z}(G^2w') = 0,$$

where the velocities u', v' are indicated in Fig. 15, w' is the axial velocity and $G = \sqrt{\sinh^2\xi + \sin^2\varphi}$.

Upon introducing the same approximations as were used for the cylindrical case, i.e. the small perturbation approximation and $w = f(z)$, the above equations reduce to:

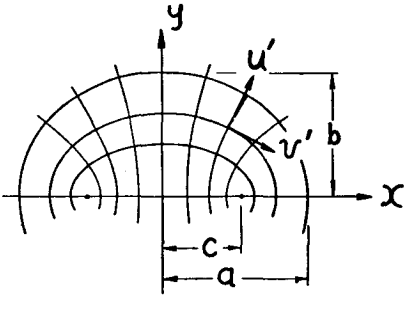

Fig. 15. The coordinate system for elliptic pipes.

$$w\frac{\partial u}{\partial z} = -\frac{1}{\rho}\frac{1}{cG}\frac{\partial p}{\partial \xi} + F_\xi \tag{25}$$

$$w\frac{\partial v}{\partial z} = -\frac{1}{\rho}\frac{1}{cG}\frac{\partial p}{\partial \varphi} + F_\varphi \tag{26}$$

$$\frac{\partial}{\partial \xi}(Gu) + \frac{\partial}{\partial \varphi}(Gv) = 0\,. \tag{27}$$

We introduce a stream function, which is a solution of the last equation above, defined by

$$u = \frac{1}{aG}\frac{\partial \psi}{\partial \varphi}\,; \qquad v = -\frac{1}{aG}\frac{\partial \psi}{\partial \xi}\,, \tag{28}$$

where a is the semi-major axis of the cross-section of the pipe. By putting this definition into (25) and (26) and eliminating the pressure by cross-differentation there results

$$\frac{\partial^2 \psi}{\partial \varphi^2} + \frac{1}{w}\left[\frac{\partial w}{\partial \varphi}\frac{\partial \psi}{\partial \varphi} + \frac{\partial w}{\partial \xi}\frac{\partial \psi}{\partial \xi}\right] + \frac{\partial^2 \psi}{\partial \xi^2} = \frac{az}{w}\left[\frac{\partial}{\partial \varphi}(GF_\xi) - \frac{\partial}{\partial \xi}(GF_\varphi)\right]. \tag{29}$$

The same assumption about the body force, as previously, is made, in that it is directly proportional to the square of the particle's velocity and indirectly proportional to the radius of curvature of the pipe. However distinction is made here between two possible cases:

1. If the body force acts parallel to the major axis of the elliptic pipe, the body force components are

$$F_\xi = \frac{w^2}{GR}\cos\varphi \sinh\xi$$

and (30)

$$F_\varphi = -\frac{w^2}{GR}\sin\varphi\cosh\xi\,.$$

2. If the body force acts parallel to the minor axis of the elliptic cross-section, its components are

$$F_\xi = \frac{w^2}{GR}\sin\varphi\cosh\xi$$

$$F_\varphi = \frac{w^2}{GR}\cos\varphi\sinh\xi\,. \tag{31}$$

Using the relations (30) in (29) we obtain

$$\frac{\partial^2 \psi}{\partial \varphi^2} + \frac{1}{w}\left[\frac{\partial w}{\partial \varphi}\frac{\partial \psi}{\partial \varphi} + \frac{\partial w}{\partial \xi}\frac{\partial \psi}{\partial \xi}\right] + \frac{\partial^2 \psi}{\partial \xi^2} = \frac{2az}{R}\left[\cos\varphi\sinh\xi\frac{\partial w}{\partial \varphi} + \sin\varphi\cosh\xi\frac{\partial w}{\partial \xi}\right] \tag{32}$$

and with relations (31) equation (29) becomes

$$\frac{\partial^2 \psi}{\partial \varphi^2} + \frac{1}{w}\left[\frac{\partial w}{\partial \varphi}\frac{\partial \psi}{\partial \varphi} + \frac{\partial w}{\partial \xi}\frac{\partial \psi}{\partial \xi}\right] + \frac{\partial^2 \psi}{\partial \xi^2} = \frac{2az}{R}\left[\sin\varphi\cosh\xi\frac{\partial w}{\partial \varphi} - \cos\varphi\sinh\xi\frac{\partial w}{\partial \xi}\right]. \tag{33}$$

If the entrance velocity distribution is known, either analytically or from experiment, then w and its derivatives will be known at each point (ξ, φ).

Under these circumstances (32) and (33) can be solved throughout the entire cross-section by the usual numerical methods.

However, if the inlet velocity has a confocal elliptic distribution, so that $\omega = \omega(\zeta)$ only, then in equations (32) and (33) further simplifications can be made so that the following equations result respectively.

$$\frac{\partial^2 \psi}{\partial \varphi^2} + \frac{1}{w}\frac{dw}{d\xi}\frac{\partial \psi}{\partial \xi} + \frac{\partial^2 \psi}{\partial \xi^2} = \frac{2az}{R}\sin\varphi\cosh\xi\frac{dw}{d\xi} \tag{34}$$

and

$$\frac{\partial^2 \psi}{\partial \varphi^2} + \frac{1}{w}\frac{dw}{d\xi}\frac{\partial \psi}{\partial \xi} + \frac{\partial^2 \psi}{\partial \xi^2} = -\frac{2az}{R}\cos\varphi\sinh\xi\frac{dw}{d\xi}. \tag{35}$$

Substitutions of the form

$$\psi_1 = c\,\sigma_1(\xi)\sin\varphi$$

and

$$\psi_2 = c\,\sigma_2(\xi)\cos\varphi$$

made in (34) and (35), respectively, reduce these partial differential equations to total differential equations. For convenience we introduce also the following dimensionless parameters:

$\beta = \dfrac{w}{w_0}$ where w_0 is the maximum value of the inlet-velocity distribution.

$\eta = \dfrac{\xi}{\xi_0}$ where ξ_0 defines the outside of the elliptic cross-section.

$\delta = \dfrac{z}{a}$; $\quad \lambda = \dfrac{a}{R}$

$$\frac{\psi_1}{\delta\lambda a w_0} = \sigma_1(\eta)\sin\varphi, \text{ in (34)}; \qquad \frac{\psi_2}{\delta\lambda a w_0} = \sigma_2(\eta)\cos\varphi, \text{ in (35)}.$$

The resulting equations are

$$\frac{d^2\sigma_1}{d\eta^2} + \frac{1}{\beta}\frac{d\beta}{d\eta}\frac{d\sigma_1}{d\eta} - \xi_0^2\sigma_1 = 2\xi_0\frac{d\beta}{d\eta}\cosh(\xi_0\eta) \tag{36}$$

and

$$\frac{d^2\sigma_2}{d\eta^2} + \frac{1}{\beta}\frac{d\beta}{d\eta}\frac{d\sigma_2}{d\eta} - \xi_0^2\sigma_2 = -2\xi_0\frac{d\beta}{d\eta}\sinh(\xi_0\eta). \tag{37}$$

The boundary conditions to be satisfied by the solutions of these equations are

$$\sigma_1(0) = \sigma_2(0) = 0$$
$$\sigma_1(1) = \sigma_2(1) = 0.$$

With the inlet-velocity distribution, i.e. $\beta(\eta)$ known, the solution of (36) and (37) can be obtained, as was done for the circular pipe case, in the form of a finite power series in η, simply by satisfying the differential equation in a finite number of points.

Assuming finite power series solutions of the form

$$\sigma_1(\eta) = \sum_1^n b_k \eta^k; \qquad \sigma_2 = \sum_1^n c_k \eta^k,$$

the stream functions for the secondary flow in the elliptic pipes appear respectively as

$$\psi_1 = \lambda \delta a w_0 \sum_1^n b_k \eta^k \sin \varphi$$

and

$$\psi_2 = \lambda \delta a w_0 \sum_1^n c_k \eta^k \cos \varphi .$$

From these stream functions the secondary flow velocity components are found by using the definitions (28) to be

$$u_1(\eta, \varphi) = \frac{\lambda \delta w_0}{G} \sum_1^n b_k \eta^k \cos \varphi ,$$

$$v_1(\eta, \varphi) = -\frac{\lambda \delta w_0}{\xi_0 G} \sum_1^n k b_k \eta^{k-1} \sin \varphi ;$$

and

$$u_2(\eta, \varphi) = -\frac{\lambda \delta w_0}{G} \sum_1^n c_k \eta^k \sin \varphi$$

$$v_2(\eta, \varphi) = -\frac{\lambda \delta w_0}{\xi_0 G} \sum_1^n k c_k \eta^{k-1} \cos \varphi .$$

These velocity components permit the vorticity in the plane of the cross-section of the pipe to be evaluated, which is respectively for the two cases considered above:

$$\gamma_1(\eta, \varphi) = \frac{\lambda \delta w_0}{c G^2} \sum_1^n b_k \left(\eta^k - \frac{k(k-1)}{\xi_0^2} \eta^{k-2} \right) \sin \varphi$$

and

$$\gamma_2(\eta, \varphi) = \frac{\lambda \delta w_0}{c G^2} \sum_1^n c_k \left(\eta^k - \frac{k(k-1)}{\xi_0^2} \eta^{k-2} \right) \cos \varphi .$$

The same sort of analysis, as used above, can be applied equally well to pipes of arbitrary cross-section. However, when the inlet-velocity distribution exhibits no symmetrical properties in terms of the chosen coordinates, simplifications in the differential equation for the stream function of the secondary flow, as obtained above, cannot be made.

Chapter V. Application of the Theory

Using the theory developed for a bent circular pipe, as presented in § 2, Chapter IV, a numerical application is made and compared with experiment. The specifications of the bent pipe considered correspond to pipe I, described previously as having a diameter of 10 cm, a radius of curvature of 273 cm and an angle of bend of 21 degrees. The inlet-velocity distribution $\beta(\eta)$ was taken from the measured distribution B. The theoretical inlet-profile is the symmetrical average value of distribution B. This theoretical curve is terminated on the wall of the pipe at an axial-velocity ratio of $w/\overline{w} = 0.80$, see Fig. 17, thus ignoring the region of large velocity gradient. This is in accordance with the assumption made in developing the theory.

The solution of equation (19) for obtaining $\sigma(\eta)$ was carried out using the procedure explained in Chapter IV. For this approximate solution the equation was satisfied uniquely at the points $\eta = 0$, 0.2, 0.4, 0.6, 0.8, and 1.0. Since the theoretical inlet-velocity distribution has a zero slope at $\eta = 0$, the coefficient $a_2 = 0$. Thus there resulted $j + 1 = 6$ algebraic equations. The finite power series solution for $\sigma(\eta)$ will contain six terms of ascending powers of η with the term η^2 missing. The simultaneous solution of these six algebraic equations yielded the six constant coefficients for the finite series expansion of the secondary flow stream function. The stream function for this case is:

$$\psi = \theta r_1 w_0 [-0.1376\,\eta + 0.1061\,\eta^3 + 0.2076\,\eta^4 - 0.4070\,\eta^5 + 0.2257\,\eta^6 + 0.0052\,\eta^7] \cos\varphi .$$

The streamlines given by this stream function are plotted in Fig. 16. The shape of these curves is similar to those obtained in Chapter II, and also confirms the suggested streamlines of the physical argument in Chapter I.

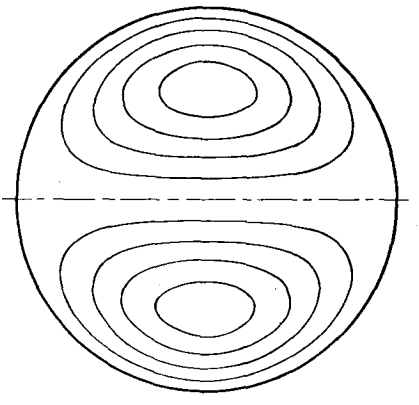

Fig. 16. The secondary flow streamlines due to inlet-velocity distribution B with $(w/\overline{w})_{wall} = 0.80$.

The secondary flow velocities obtained from this stream function were then applied, according to equations (22), to calculate their effect on changing the shape of the axial-velocity distribution. In this step-wise calculation around the bend to 21 degrees, the axial-velocity distribution was computed at the stations $\theta = 5°$, 10°, 13°, 16°, 19°, and 21°. At each cross-section, one iteration was used to obtain a more accurate average of the quantities indicated in (22).

The variation of the shape of axial-velocity distribution as the flow moves around the bend can seen from the results plotted in Figs. 17 and 18. Clearly, the deformation begins slowly, being small for small angles, but increases sharply for larger angles of bend. This results from the fact that the displacement of a particle is a function of the square of the distance from the inlet, measured along the longitudinal axis. The resulting velocity distribution after a bend of 21 degreees is shown in Fig. 17. For comparison purposes the measured velocity distribution has been plotted on the same figure. The comparison shows that the results of this theory are in good agreement with the experimental results. The curves of constant velocity in the higher velocity region are of the correct shape. The regions defined by the theoretical curves of constant velocity have not increased in area, but have merely changed in shape, since no variation of the particle's axial-velocity magnitude has been considered. The corresponding regions, defined by the measured curves, exhibit an increase in area due to the growth of the boundary layer, which causes an acceleration of the fluid in the central region of the pipe. The curves of constant velocity in the lower velocity region, while having the correct shape in the region of the cross-section on the outside of the bend, do not exhibit the indentations on the inside of the bend as do the measured curves. It will be shown, however, that this characteristic can also be obtained from the theory.

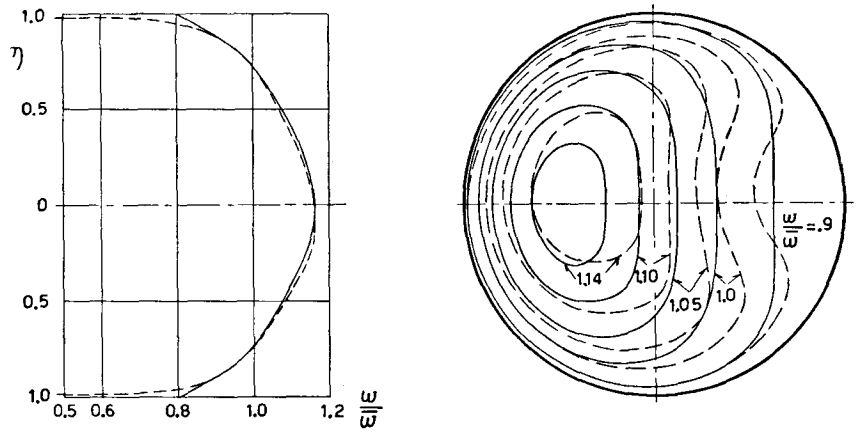

(a) (b)

Fig. 17. Theoretical (solid) and measured (dashed) lines of constant axial velocity at the exit of: (b), pipe I, with a bend angle of 21 degrees, resulting from (a), inlet ristribution B, where $\overline{w} = 4160$ cm/sec. and $(w/\overline{w})_{wall} = 0.80$.

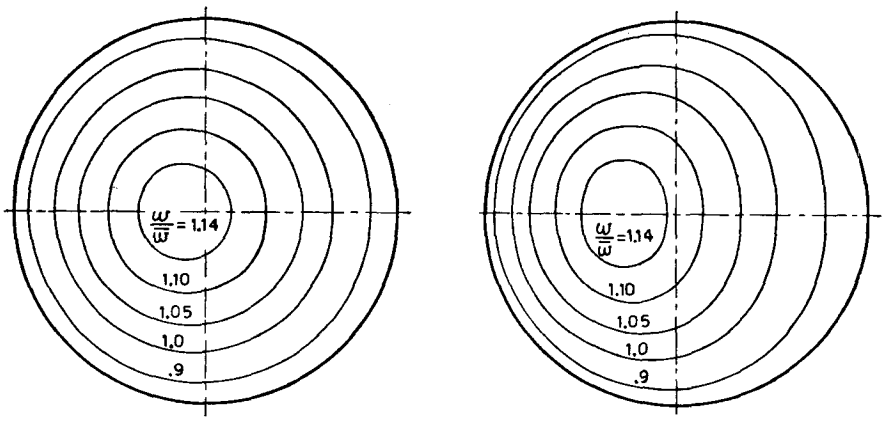

(a) (b)

Fig. 18. Calculated lines of constant axial velocity in pipe I at: (a), 10 degree bend angle, and (b), 16 degree bend angle resulting from inlet distribution B with $(w/\overline{w})_{wall} = 0.80$.

As a check of the validity of the assumption that the secondary flow velocities be small compared to the axial velocity, the following results are given. The maximum value of the radial velocity component occurs at $\eta = 0$ and $\varphi = 90°$. The maximum value of the tangential velocity component occurs at $\eta = 1$ and $\varphi = 0°$. The resulting equations are

$$\max \left| \frac{u}{w_0} \right| = 0.1376\,\theta$$

$$\max \left| \frac{v}{w_0} \right| = 0.3665\,\theta\,.$$

These equations evaluated at $\theta = 21°$ give the following values:

$$\max \left| \frac{u}{w_0} \right|_{\theta = 21°} = 5.04\%$$

$$\max \left| \frac{v}{w_0} \right|_{\theta = 21°} = 13.43\%.$$

Thus we see from the maximum value of the tangential velocity at a 21 degree bend angle, the upper limit of the small perturbation approximation is being approached.

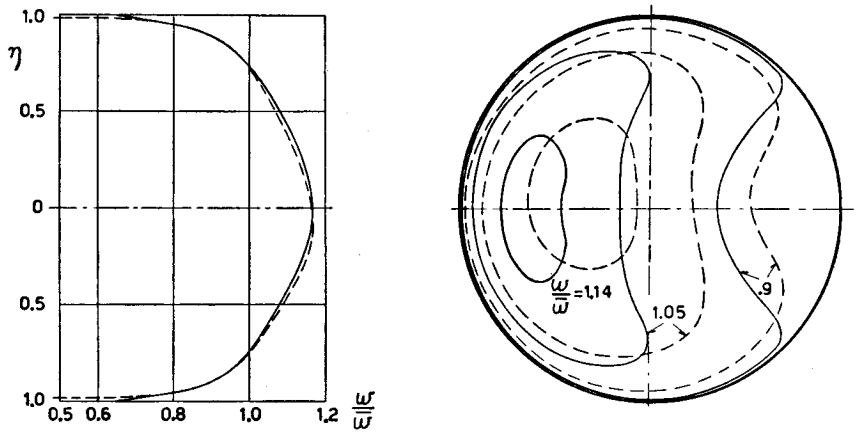

(a) (b)

Fig. 19. Theoretical (solid) and measured (dashed) lines of constant axial velocity at the exit of: (b), pipe I, with a bend angle of 21 degrees, resulting from (a), inlet distribution B, where $\bar{w} = 4160$ cm/sec. and $(w/\bar{w})_{wall} = 0.65$.

To show that the indentations exhibited by the experimental curves on the inside of the bend can be obtained from the theory, the following calculation was made. The assumed inlet-velocity distribution was the same as used for the above example except that it was terminated on the wall of the pipe at a velocity ratio of $w/\bar{w} = 0.65$, see Fig. 19. By making this variation we are essentially taking into consideration a portion of the boundary-layer gradient. The solution for the secondary flow stream function, obtained by satisfying (19) in the same points as for the example above, is

$$\psi = \theta r_1 w_0 [-0.2201\,\eta + 2.3516\,\eta^3 - 11.8122\,\eta^4 + 24.3487\,\eta^5 - 22.1641\,\eta^6 + 7.4961\,\eta^7] \cos\varphi.$$

This secondary flow solution was used to calculate the change of the axial-velocity distribution due to the bend, the resulting distribution at a bend angle of 21 degrees being shown in Fig. 19. Obviously, the theoretical curves are excessively displaced, but the general character of these curves is correct. With the assumed inlet-velocity distribution, for this example, consideration has been given to a portion of the bondary layer, that is a small region of high

velocity gradient on the wall. This resulted in larger secondary flow velocities and hence a larger distortion of the axial-velocity distribution. We know, however, that the viscous forces become large under these circumstances of large velocity gradients and they would therefore resist the effects of the secondary flow. However, the theory is based on the inviscid fluid approximations so that this resisting effect is not included. We can conclude that these indentations of the constant velocity curves on the inside of the bend have their origin from the effect of the fluid in the high velocity gradient region close to the wall. As shown by the previous example, the theory gives good results if the large velocity gradient of the entrance velocity distribution is neglected, as was originally assumed in the theoretical development.

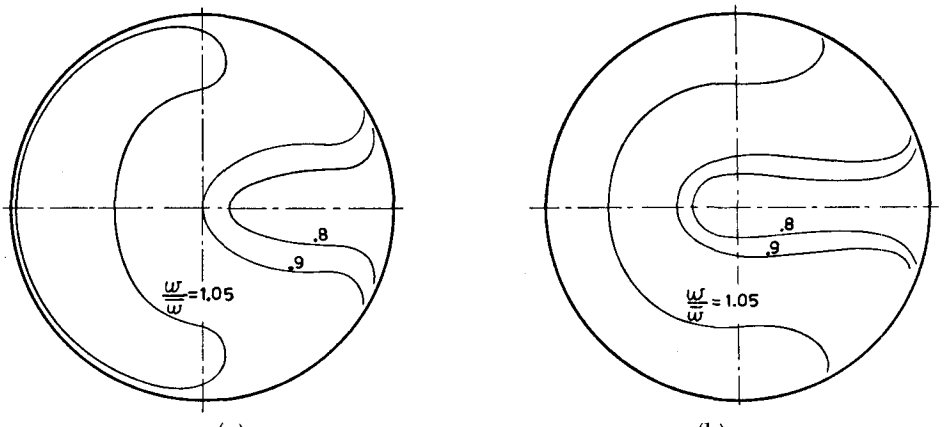

(a) (b)

Fig. 20. Calculated lines of constant axial velocity in pipe I at: (a), 25 degree bend angle, and (b), 28 degree bend angle resulting from inlet distribution B with $(w/\bar{w})_{wall} = 0.65$.

To show that the theory will produce well defined regions of low velocity fluid on the inside of the bend, this calculation was carried out for bend angles larger than 21 degrees. The resulting axial velocity distributions for bend angles of 25 and 28 degrees are shown in Fig. 20. The shape of the constant velocity curves display the general shape of the experimental curves obtained from the tests on pipe II, in that the regions of low axial-velocity are well defined, and the curves are showing the tendency to form closed regions of this low axial-velocity fluid.

From the above numerical examples and the comparison of the results with experiment it can be concluded that an important factor for the secondary flow phenomenon within a bend is the axial-velocity distribution upstream of the bend. Since in the theoretical development only the inlet axial-velocity distribution was used to determine the secondary flow rather than the local axial-velocity distribution, the results are applicable only for small angles of bend, i.e. the initial phases of the secondary flow, where the local velocity profile is not greatly different from that one at the inlet of the curved pipe. The examples above show that the theory does produce constant axial-velocity curves in the bend of the pipe of the correct shape and approximately the

correct displacement if proper respect is given to the approximations that are made. In particular, the region of high velocity gradient near the wall of the pipe, as is present with a turbulent velocity profile, must be omitted from the theoretical inlet velocity distribution.

It is to be noted that the stream function for the secondary flow, as obtained here, is a linear function of the angle of bend. This might lead one to believe that this same stream function could be used for a pipe of arbritary radius of curvature. However it must be remembered that the theory is applicable only for pipes whose cross-sectional dimensions are small compared to the radius of curvature.

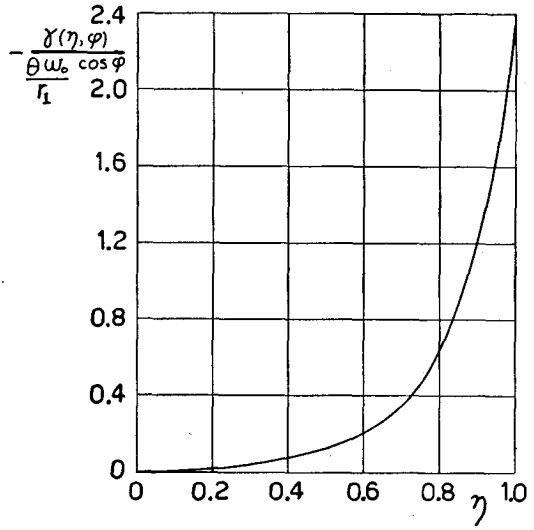

Fig. 21. The vorticity distribution due to the secondary flow in pipe I resulting from inlet distribution B, with $(w/\overline{w})_{wall} = 0.80$.

In general, this theory shows the extent to which a first order "ideal fluid" theory can be used to calculate the secondary flow in a slightly bent pipe. Improvements could of course be expected from a second order theory in which the effect upon the secondary flow of the local stagnation pressure distribution within the bend is taken into consideration.

It is of interest to investigate the vorticity distribution that results from the secondary flow velocities obtained in the above example. Having the constant coefficients as obtained for the series solution for the secondary flow stream function, we simply apply the equation for the vorticity distribution as developed in Chapter IV. The dimensionless vorticity resulting for the first example above, which has an axial-velocity ratio on the wall of the pipe of $w/\overline{w} = 0.80$, is shown in Fig. 21.

Chapter VI. The Losses Due to the Secondary Flow

§ 1. The Loss Coefficient and its Application

Since fluid with a non-uniform axial-velocity flowing in a curved pipe gives rise to a secondary flow, whereas there was no secondary flow at the entrance of the bend, it represents a certain loss of energy from the principal axial flow. With respect to the friction losses, there appears within the cross-section a given distribution of those losses. A result of the faster moving particle displacing toward the outside of the bend is to increase the axial-velocity gradient in this region while decreasing the gradient on the inside of the bend. Therefore, the dissipation due to the viscous forces will be larger in the cross-section of the pipe toward the outside of the bend than those on the inside of the bend. Apart from the viscous forces, the energy in the secondary flow can be considered as a loss, in which we shall be interested here. The dissipation of energy due to the secondary flow, when considered independent of the friction losses, can be thought of as an induced drag similar to that obtained from wing theory.

The energy passing through each cross-section of the pipe per unit time must be a constant. The energy consists of the kinetic energy plus the work of the surface forces. Thus we can write

$$\int_A \left[p + \frac{\rho}{2}(w^2 + u^2 + v^2) \right] w \, dA = \text{const.}$$

Since it was assumed that the axial velocity does not change its magnitude as the fluid moves around the bend the kinetic energy of the axial flow is also constant. If the above integral is evaluated between the inlet to the bend and a cross-section in the bend the kinetic energy of the axial flow gives no contribution to the resulting value, that is

$$\int_1^2 \frac{\rho}{2} w^3 \, dA = 0 ,$$

where the limit 1 indicates the inlet and 2 any arbritary cross-section in the bend.

Thus we see from the first integral above, the energy in the secondary flow corresponds to a pressure drop. From the pressure difference calculated between the inlet cross-section and any arbritary cross-section in the bend, a secondary flow loss coefficient is defined by

$$\zeta = \frac{\Delta p}{\rho/2 \, \overline{w}^2} = \frac{1}{\rho/2 \, \overline{w}^3 A} \int_A \frac{\rho}{2} [u^2 + v^2] \, w \, dA$$

where A = area of the cross-section

w, u, v = velocity components at the cross-section in question.

$\overline{w}$ = average mass-flow velocity $= \frac{1}{A} \int_A w \, dA$.

The above equation for the loss coefficient, written in terms of the variables introduced for the circular pipe, is

$$\zeta = \frac{\theta^2 w_0^2}{\pi \overline{w}^3} \int_0^{2\pi} \int_0^1 \left[\left(\frac{\sigma}{\eta} \sin \varphi \right)^2 + \left(\frac{d\sigma}{d\eta} \cos \varphi \right)^2 \right] w \eta \, d\eta \, d\varphi .$$

The loss coefficient for the first theoretical example given has been calculated. With the downstream section taken at an angle of bend of 21 degrees, the calculated loss coefficient indicates the loss due to the secondary flow from the entrance to this cross-section. The theoretical values of the velocities, obtained at the station $\theta = 21°$, were used in the integration indicated above. The integration was carried out numerically using Simpson's rule. The number of points in the cross-section used was 360. The resulting value of ζ is 0.00253.

The calculation was repeated, but here the inlet-velocity distribution was used instead of the local axial-velocity distribution obtained at a bend angle of 21 degrees. All other values in the integration remained the same. Since the inlet-velocity distribution is symmetrical about the longitudinal axis, the integration with respect to the variable φ can be evaluted analytically. Therefore the numerical method is required only for the integration with respect to η. Hence the amount of computations, to evaluate the integral, are greatly reduced. The loss coefficient resulting from this calculation is 0.00249. The difference of this value from that obtained above is small, being 1,6%, so that, for small angles of bend, loss calculations using this simplified method give a good approximation to the exact value.

These losses which represent the energy in the secondary flow are relatively small. *Eichenberger* [12] found by measuring the secondary flow velocities in a curved square pipe that after a 90 degree bend angle the energy in the secondary flow is only about 1% of the energy in the principal flow. Comparing the calculated values with the measured pressure drop in pipe I from which $\Delta p/\overline{q} = 0.016$, we see the energy of the secondary flow represents only about 15% of the total loss. This then indicates that the dissipation due to viscosity plays a more important role in the bend losses of a constant-area curved pipe than the energy in the secondary flow. It can be seen that this viscous dissipation has a definite distribution within the cross-section of the pipe. Because of the increased gradient of the stagnation pressure distribution toward the outside of the bend the viscous dissipation in this region will also be increased and hence a greater portion of the viscous losses will occur in the region toward the outside of the bend. This increased gradient represents an increased viscous dissipation with respect to the axial flow. In addition of course there occur viscous losses due to the secondary motion in the plane of the cross-section.

For the case of a curved diffusor, which would be an interesting continuation of the study of secondary flows, the relative importance of the secondary flow energy and the viscous dissipation may be reversed from the case of a constant-area pipe. Since the size of the cross-section grows larger as the flow moves around the bend, there is more opportunity for the velocities in the plane of the cross-section to become larger. Thus the energy in this motion would show a corresponding increase. At the same time, with the simultaneous variation due to both the enlarging cross-section and the secondary motion, the viscous

dissipation due to the variation of the stagnation pressure distribution gradient may not increase as rapidly. In this case the energy in the secondary motion would be the predominant factor of the bend losses. Thus an inviscid fluid theory for the secondary flow in curved diffusors could perhaps predict the actual bend losses more closely than the inviscid fluid theory for curved constant-area pipes.

The losses calculated above represent only those secondary flow losses which occur in the bend of the pipe. However, since the secondary flow has been initiated, it will continue, even though the pipe is no longer curved, until it is dissipated by friction. Therefore, in addition to the losses within the bend itself, appreciable viscous losses due to the secondary flow can occur downstream of the bend. *Wasielewski* [8] measured the secondary flow losses in a curved circular pipe between the stations 9 diameters upstream of the bend and 50 diameters downstream and found the losses vary linearly with the bend angle up to an angle of $22^1/_2$ degrees. The measured secondary flow loss in pipe I, which corresponds to a bend angle of 21 degrees, is slightly less then one half of the value found by *Wasielewski*. This indicates the losses downstream of the bend can be as important and worthy of consideration as the losses within the bend.

§ 2. The Loss in Circular and Elliptic Pipes

It is of interest to compare the secondary flow losses in pipes of different cross-sections. For the present discussion we consider a circular pipe and a differently oriented elliptic pipe. It is quite easy to see which of these pipes will have the greatest loss due to the secondary flow. As was seen from the study of the secondary flow in a circular pipe, the effect was to displace the circular lines of constant stagnation pressure towards the outside of the bend and at the same time distort these lines from their circular shape. The displacement of these lines is a function of the secondary flow velocities. For discussional purposes consider the analogical problem of two co-axial circular cylinders where the inner cylinder is suddenly made to move tangentially with a given velocity. It will experience a certain resisting force due to its apparent mass. Now if these cylinders are elliptical in cross-section obvious differences result. The apparent mass of an elliptic cylinder moving parallel to its major axis is smaller than when it moves parallel to its minor axis. Therefore, the resisting force, due to the apparent mass, experienced by the elliptic cylinder moving parallel to its major axis inside of another elliptic cylinder is smaller than if this motion were parallel to the minor axis. Hence under the action of a given disturbing force, which for motion in curved pipes corresponds to the centrifugal force, the elliptic cylinder moving parallel to its major axis will move faster than the cylinder moving parallel to its minor axis. Carrying this analogy over to the flow in curved pipes, the motion of the internal cylinder gives a measure of the secondary flow velocities. Thus the case of a bent elliptic pipe oriented with its major axis lying in the plane of the bend will have the larger secondary velocities of the two cases considered here and hence will have the greater secondary flow losses.

For comparison purposes the secondary flow losses in a circular and an elliptic pipe are made. The inlet-velocity distribution used for the circular pipe

was parabolic in shape. The velocity on the wall of the pipe was taken as 0.7 of its maximum value in the center.

The elliptical cross-section used had a major axis to minor axis ratio of 2:1. The confocal elliptic inlet-velocity distribution had the same maximum and wall value as used for the circular pipe. The area was chosen so that the average mass flow velocity was the same as that of the circular pipe. This resulted in the ratio $r_1/a = 0.740$, where r_1 is the radius of the circular pipe and a is the semi-major axis of the elliptic pipe.

To different cases were considered for the elliptical pipe. For the first case, the pipe was oriented so that the centrifugal force acted parallel to the major axis of the ellipse. For the second case the centrifugal force acted parallel to the minor axis of the ellipse. The secondary flow solutions were obtained by satisfying the respective differential equations uniquely at $\eta = 0$, 0.25, 0.50, 0.75, and 1.0, yielding a five term series solution. The loss coefficient calculations were made using the inlet axial velocity distribution as discussed in § 1.

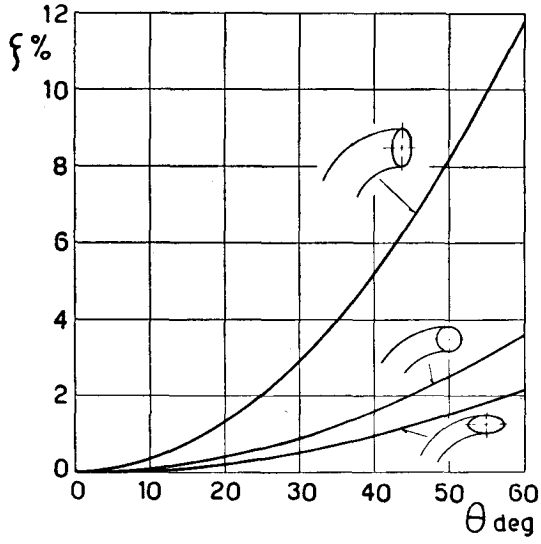

Fig. 22. Calculated secondary flow loss *vs* angle of bend for circular and elliptic pipes with $(w/\overline{w}_0)_{wall} = 0.70$.

The results of these calculations are plotted in Fig. 22. All of the loss coefficient curves are parabolic since the loss is proportional to the square of the angle of bend. The losses due to the secondary flow in the elliptic pipe oriented with its major axis parallel to the centrifugal force are approximately $5^1/_2$ times as great as those for the elliptic pipe oriented with its minor axis parallel to the centrifugal force. A knowledge of this information can be employed to good advantage when pipes of non-circular cross-section are used in an installation. A general rule can be stated: The secondary flow losses in a curved pipe of arbritary cross-section but fixed radius of curvature and angle of bend can be minimized by orienting the pipe so that its largest cross-sectional dimension is perpendicular to the line of action of the centrifugal force.

These ideas have been used in the design of the passages in the diffusor section of centrifugal compressors, since it was found, from experience, that the use of non-circular passages oriented according to the above rule increased the efficiency of these compressors.

Appendix A. Convergence of the Method of Solution for the Secondary Flow

The convergence characteristics of the method for integrating the differential equation satisfied by the secondary flow are demonstrated. The method involves satisfying the differential equation uniquely at a finite number of points within the interval of integration. This procedure yields a system of algebraic equations. The number of unknowns in these equations is the same as the number of equations. The simultaneous solution of the system of equations produces the constant coefficients used in the finite series expansion of the solution of the differential equation.

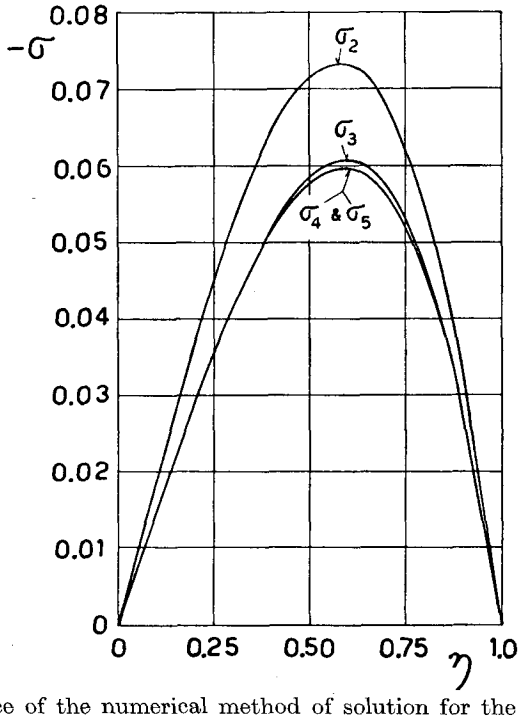

Fig. 23. Convergence of the numerical method of solution for the secondary flow in a bent circular pipe.

For this demonstration, a circular pipe is considered. The symmetrical inlet-velocity distribution is parabolic in shape, having a velocity value on the wall equal to 0.7 of its maximum value in the center of the pipe, i. e. $\beta(\eta) = 1 - 0.3\,\eta^2$.

Using this inlet-velocity distribution, solutions of equation (19) are obtained as follows:

a) Satisfying the differential equation at $\eta = 0$ and $\eta = 1.0$ yields

$$\sigma_2(\eta) = -0.1909\,\eta + 0.1909\,\eta^3.$$

b) Satisfying the differential equation at $\eta = 0$, 0.5, and 1.0 yields

$$\sigma_3(\eta) = -0.1488\,\eta + 0.1058\,\eta^3 + 0.0430\,\eta^4.$$

c) Satisfying the differential equation at $\eta = 0$, 0.33, 0.67, and 1.0 yields

$$\sigma_4(\eta) = -0.1511\,\eta + 0.1507\,\eta^3 - 0.0305\,\eta^4 + 0.0309\,\eta^5.$$

d) Satisfying the differential equation at $\eta = 0$, 0.25, 0.50, 0.75, and 1.0 yields

$$\sigma_5(\eta) = -0.1505\,\eta + 0.1335\,\eta^3 + 0.0214\,\eta^4 - 0.0230\,\eta^5 + 0.0186\,\eta^6.$$

These solutions are plottes in Fig. 23. The solutions converge rapidly as the number of matching points is increased.

The example shows, that with a smooth inlet-velocity distribution, the number of matching points required is relatively small. In this case the five points used to obtain the last solution are sufficient. However, if the entrance velocity is not so smooth as the one used here, the number of matching points necessary will probably increase.

Literature References

1. *J. Thomson:* Experimental Demonstration in Respect to the Origin of Wingings of Rivers in Alluvial Plains. Proc. Roy. Soc., Lond. Vol. 26 (1877), pp. 356—357.
2. *W. R. Dean:* The Streamline Motion of Fluid in a Curved Pipe. Phil. Mag. (7), Vol. 4 (1927), p. 208 and Vol. 5 (1928), p. 673.
3. *C. M. White:* Streamline Flow through Curved Pipes. Proc. Roy. Soc., Lond. (A), Vol. 123 (1929), p. 645.
4. *M. Adler:* Strömung in gekrümmten Rohren. Z. ang. Math. u. Mech., Vol. 14 (1934), p. 257.
5. *H. Nippert:* Über den Strömungswiderstand in gekrümmten Kanälen. Forsch.-Arb. Ing.-Wes. Nr. 320 (1929).
6. *H. Nippert:* Neuere Versuche über den Strömungsvorgang in gekrümmten Kanälen. Der Bauingenieur, Vol. II, pp. 76—79, Jan. 1930.
7. *H. Richter:* Der Druckabfall in gekrümmten glatten Rohrleitungen. Forsch.-Arb. Ing.-Wes. Nr. 338 (1930).
8. *R. Wasielewski:* Verluste in glatten Rohrkrümmern mit kreisrundem Querschnitt bei weniger als 90° Ablenkung. Mitteilungen des Hydraulischen Instituts der Tech. Hochschule München. (1932) Bk. 5, p. 53.
9. *G. J. Taylor:* The Criterion for Turbulence in Curved Passages. Proc. Roy. Soc., Lond. (A), Vol. 124 (1929), p. 243.
10. *H. B. Squire* and *K. G. Winter:* The Secondary Flow in a Cascade of Airfoils in a Nonuniform Stream. Journal of the Aeronautical Sciences, Vol. 18, No. 4 (1951), p. 271.
11. *W. R. Hawthorne:* Secondary Circulation in Fluid Flow. Proc. Roy. Soc., Lond. (A), Vol. 206 (1951), p. 374.
12. *H. P. Eichenberger:* Shear Flow in Bends. Office of Naval Research Technical Report No. 2, Contract N 5 ori 07848, 1952.
13. *Milne-Thompson:* Theoretical Hydrodynamics.
14. *H. Lamb:* Hydrodynamics.
15. *Dwight:* Table of Integrals.
16. *W. R. Sears:* Theoretical Aerodynamics, Part I.
17. *Margenau* and *Murphy:* The Mathematics of Physics and Chemistry.

Biography

In the year 1925 on 23 March I was born in Thompsontown, Pennsylvania, USA. My primary education was obtained by attending the public grammar and high schools in the cities of Palmyra and Lancaster, Penna. After graduation from high school in June 1943 I enlisted in the United States Navy and in November 1943 was assigned as an Officer Candidate to the University of Pennsylvania to study mechanical engineering. In November 1944 a transfer to Cornell University in Ithaca, New York, was made, where my study of mechanical engineering was continued. With the successful completion of the prescribed course of study the degree Bachelor of Science in Mechanical Engineering was awarded to me in June 1946 and at the same time I was commissioned an Ensign in the United States Navy. My next naval assignment was to the Flight Test Division of the Naval Air Test Center, Patuxent River, Maryland, where I conducted flight test projects on experimental Naval aircraft. After my release from the Navy in December 1947, I remained at the Naval Air Test Center retaining the same position but in a civilian capacity. A desire to persue further studies in aeronautics resulted in my enrollment in the Graduate School of Aeronautical Engineering at Cornell University in September 1949 and in June 1951 I was awarded the degree Master of Aeronautical Engineering. A fellowship granted by the National Research Council of Washington, D. C., made possible a continuation of my graduate studies in aeronautics at the Swiss Federal Institute of Technology, Zurich. It was during the span of this grant that I made my investigations of the secondary flow in curved pipes, under the scientific direction of Professor Dr. J. Ackeret.